LADAR Proximity Fuze - System Study -

ERIC BLANQUER

Abstract

LADAR (Laser Detection and Ranging) systems constitue a direct extension of the conventional radar techniques. Because they operate at much shorter wavelengths, LADARs have the unique capability to generate 3D images of objects. These laser systems have many applications in both the civilian and the defence fields concerning target detection and identification. The extraction of these features depends on the processing algorithms, target properties and 3D images quality. In order to support future LADAR hardware device developments and system engineering studies, it is necessary to understand the influences of the phenomena leading to the final image. Hence, the modelling of the laser pulse, propagations effects, reflection properties, detection technique and receiver signal processing have to be taken into account.

A complete simulator has been developed consisting of a graphical user interface and a simulation program. The computer simulation produces simulated 3D images for a direct detection pulse LADAR under a wide variety of conditions. Each stage from the laser source to the 3D image generation has been modelled. It yields an efficient simulation tool which will be of help in the design of the future LADAR systems and gauge their performances.

This master's thesis contains the theoretical background about laser used to build the simulation program. The latter is described schematically in order to provide an insight for the reader. The graphical interface is then presented as a short user's manual. Finally, in order to illustrate the possibilities of the simulator, a collection of selected simulations concludes the report.

Keywords: LADAR, laser radar, laser scanning, range image, pulse detection, modelling, simulation, graphical interface, Matlab.

Saab Bofors Dynamics

Saab group is a high-technology company that offers world-leading system solutions, services and products in defence, aviation, space and civil security. Saab's business operations are carried out by some fifteen business units that report directly to the group management.

Saab Bofors Dynamics is one of the business units and represents a vital part of Saab's defence activities with approximately 1100 employees. Operations at *Saab Bofors Dynamics* consist of two core activities designated as missiles and support weapons. As a consequence, *Saab Bofors Dynamics* provides complete missiles solutions. The activities, especially in the area of missiles, are technologically and productively based on the requirements and needs of the Swedish defence forces. Consequently, a close collaboration with the Swedish defence forces has been developed. On top of this, it also participates in many international collaborations.

The company's fields of expertise are: systems technology, guidance and navigation, modelling and simulation, sensor technology and warhead and propulsion technology. The sensor technology includes radar systems, optoelectronic sensors and laser technology[1]. The latter being the center of interest of this master's thesis. More precisely, the work has been done within the section of *electronics and software development (land & air defence)*, a branch of the *development and technology* department.

Saab Bofors Dynamics
Bofors industriområde
SE-691 80 Karlskoga
Sweden

---

[1]description taken from the official company presentation of 2007-01-22.

Contents

List of Figures

Part I

Background & Basis

Chapter 1

Introduction

1.1 Background

During World War II, radars used electromagnetic radiation with radio frequency ($\propto 10^{10}\ Hz$) to detect remote objects. Since that time this technique has been improved and applied to higher and higher frequencies until it reached the optical domain ($\propto 10^{14}\ Hz$). The LADARs (laser detection and ranging), or laser radars, detect targets using a laser source to produce the electromagnetic radiations. The prevalent method is to send a pulse and measure its time of flight when it arrives back at the receiver. The measured time gives an estimation of the target range for each laser shot. Such LADAR systems provide distance images and could be used as target seekers when mounted on board of missiles of type LOCAAS or E-COM.

The design of such systems implies taking into account numerous parameters and answering many questions. One may, for example, be interested in the flight altitude, the laser beam size, the range accuracy, the pulse repetition frequency or the receiver's properties. It is only possible to study independently a few of these parameters. Indeed, most of them are interconnected making the work complicated and fastidious. Thus a simulation is the appropriate means to handle these complexities and might be of help in future systems designs. However, such a wide simulator covering all the phenomena from the laser source to the receiver does not exist.

1.2 Objectives

To tackle this lack, a simulator which permits the user to tune numerous parameters and then be able to see their different influences is built. However, this simulator being the first to be developed, it has to be concise and focus on the main effects and parameters.

The purpose of this master's thesis is to develop a simulation model that will be used in LADAR systems design to carry out studies about the influences of the main parameters. At the same time, a graphical user interface will be added to the

3

simulation to facilitate its use. The final outcome will then be a LADAR simulator.

1.3   Thesis Outline

The master's thesis is made up of three parts. The first one covers the background about lasers and LADARs. It includes an introduction and the laser theory used in the simulation. The second part focuses on the main concepts of the simulation implementation and gives a description of the graphical user interface. Part 3 concludes the report by presenting the possibilities of the simulator and by showing a collection of selected results. Finally, some discussions about the conclusions and future ideas for extensions of this work are exposed.

Chapter 2

Laser Beam Propagation Theory

In order to understand the work contained in this master's thesis, the reader should be familiar with laser. This chapter describes the main aspects of laser theory and more particularly its application in LADAR systems.

The process is subdivided in four parts as shown in Figure 2.1, taken from [1]. The chapter structure follows this decomposition. Firstly, the laser method is reviewed. Secondly, the next section focuses on the laser source and describes the energy distribution of the beam (number **1**). Next, the modelling of the propagation in the atmosphere is explained (number **2**). Then, the interactions with the target are presented: the modelling of the target is described before explaining how the reflection phenomenon works (number **3**). Finally, the receiver model is exposed (number **4**) and the LADAR range equation derivation concludes this chapter.
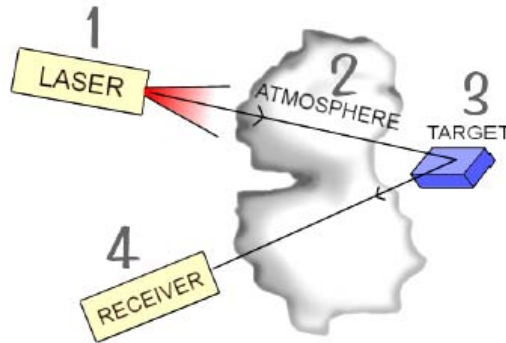
Figure 2.1. Process decomposition.

2.1   Laser Method and Range Finding Principle

The principle of the laser range finder is shown in Figure 2.2 (figure directly inspired from [2]). A laser pulse is sent out from the laser source transmitter and travels in
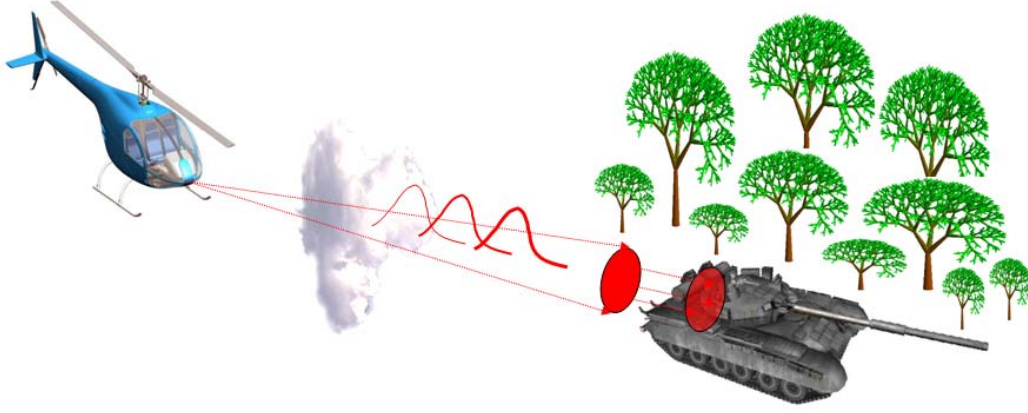
Figure 2.2. Laser range finding principle.

the air. The pulse is then reflected on a surface element which can be the target, the ground or an object. The reflected pulse is collected by the receiver and corresponds to the received signal. Thus the pulse travels twice the distance to the target: turn and return. Finally, knowing that the pulse travels at the celerity of the light and measuring the time of flight of the pulse, one computes the distance to the surface element using the formula:

$$d_{target} = \frac{\Delta t \cdot c}{2} \qquad (2.1)$$

where d_{target} is the distance from the laser source to the target, Δt is the time of flight of the pulse (round trip time) and c the celerity of the light.

2.2   Energy Distribution: Space and Time

To be able to describe the phenomenon, the laser pulse has to be modelled in time (1 dimension) as well as in space (3 dimensions) which leads to a 4 dimensions model. Fortunately, the pulse is separable in a temporal and a spatial distribution. They are together expressed as the intensity $U(x, y, z)$ where x and y are the vertical and horizontal cross-range dimensions and z is the range dimension (the direction that the pulse is travelling). These three variables (x, y, z) are shown in Figure 3.5. The expression can be found in [1, 3, 4] as follow:

$$\begin{aligned} U(x, y, z) &= V(z) \times I(x, y) \\ &= V(ct) \times I(x, y) \\ &= I_0 \cdot p(t) \times I(x, y), \end{aligned} \qquad (2.2)$$

where I_0 is the total pulse power; $I(x, y)$ is the proportion of energy contained within a component located at (x, y); $p(t)$ is the discrete pulse shape in the range

dimension. The integrals of $I(x, y)$ and $p(t)$ are both equal one because they are normalized to unity. x, y, and z ($\Leftrightarrow t$) take on discrete values.

The next two sections specify the terms in Equation (2.2). Section 2.2.1 refers to $I(x, y)$, which is the spatial distribution of the energy, namely the *irradiance* and Section 2.2.2 describes the temporal energy distribution of the pulse, $p(t)$.

2.2.1 Spatial Distribution: Irradiance Function

The intensity of an optical beam is not constant across its diameter at all ranges, see Figure 2.3 taken from [5]. The irradiance corresponds to the power of electromagnetic radiation incident on a surface and has the unit of (W/m^2). It represents the energy profile of the laser beam in the space. This profile depends on the technique used to generate the laser light (diode lasers, solid state lasers, micro-chips lasers...). However, the shape of the emmitter has more influence on this energy profile. In the LADAR simulation, the laser light is obtained from a semi-conductor laser diode which its emitting area is a slit. Before describing its model, the preliminary step is to derive the model of the most common case where the profile is Gaussian.

The Gaussian Model

The Gaussian profile is obtained from a transmitted beam that uniformly illuminates a *circular* output aperture. That case is shown in Figure 2.3 and the irradiance follows the expression developed in [5]:

$$I(r) = I_0 \exp\left(\frac{-2r^2}{\omega^2}\right), \qquad (2.3)$$

where the variable r is the distance measured, in a transverse plane, from the central axis of propagation z. ω is the beam half-width and represents an arbitrary
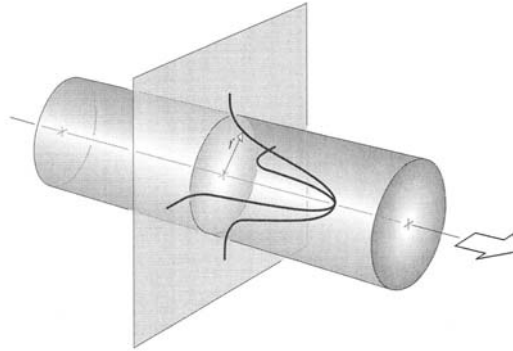
Figure 2.3. A Gaussian beam.

boundary to the beam's width. By definition, at $r = \omega$, the beam's irradiance is $I_0/e^2 = 14\% \cdot I_0$ and most of the energy resides within this imaginary cylinder of radius ω as represented in Figure 2.3. Moreover, this figure shows also the function $I(r)$ of Equation (2.3).

The Source Diode Model

The dimensions of the emitting area of the semi-conductor laser diode are so that its length is 100 times bigger than its width, typically 200 μm$\times$ 2 μm. Consequently the output aperture is not circular anymore and the model has to be adapted. The LADAR simulation is based on the model taken from [6] and is called the source diode model:

$$I(\theta_x, \theta_y) = I_0. \exp\left[-2(\left(\frac{\theta_x}{\alpha_x}\right)^{2G_x} + \left(\frac{\theta_y}{\alpha_y}\right)^{2G_y})\right], \qquad (2.4)$$

where α_x is the xz divergence angle (half divergence angle in the xz-plan), G_x is the "super Gaussian" factor for the x direction and has to be greater than 1.0. Similar definitions apply for the y subscripted values. Note that the typical Gaussian distribution is obtained when $G_x = G_y = 1.0$. An example of profile is given Figure 2.4.

Most laser diode manufacturers specify the far field divergence angles as the full width of the distribution between the half power points, θ_{FWHM}. In order to use the right coefficient α_i, one may apply the following conversion:

$$\alpha_i = (0.8493218) \cdot \theta_{FWHM,i}$$

It is well known that the laser light is highly directional. However, due to the divergence angles, the laser footprint will not have the same size at any range from the laser source. It depends on the distance: increasing the distance will increase its size. Consequently, it is sometimes handier to rewrite Equation (2.4) using the following:

- in Figure 3.5, one sees that at target range: $z = R$ and then

$$\theta_x = \arctan(\frac{x}{R})$$

- under the assumption that $R >> x$, it yields:

$$\theta_x = \frac{x}{R} - \frac{1}{3} \times \left(\frac{x}{R}\right)^3 + \dots$$

Hence, the Equation (2.4) can be rewritten as:

$$I(x, y, R) = I_0 \cdot \exp\left[-2(\left(\frac{x}{R \cdot \alpha_x}\right)^{2G_x} + \left(\frac{y}{R \cdot \alpha_y}\right)^{2G_y})\right], \qquad (2.5)$$

where (x, y) are the cross-range dimensions at a distance $z = R$.

To complete the model, the values $G_x = 1$ and $G_y = 5$ have been used in Equation (2.5) and this leads to the expression used in the LADAR simulation:

$$I(x, y, R) = I_0 \cdot \exp\left[-2\left(\left(\frac{x}{R \cdot \alpha_x}\right)^2 + \left(\frac{y}{R \cdot \alpha_y}\right)^{10}\right)\right], \qquad (2.6)$$

or equivalently

$$I(\theta_x, \theta_y) = I_0 \cdot \exp\left[-2\left(\left(\frac{\theta_x}{\alpha_x}\right)^2 + \left(\frac{\theta_y}{\alpha_y}\right)^{10}\right)\right] \qquad (2.7)$$
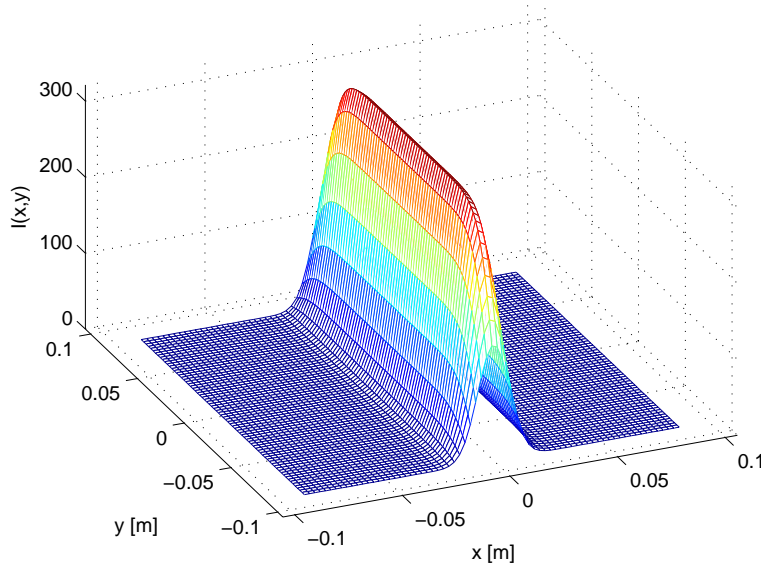
Figure 2.4. Normalized irradiance at a distance of 50 m.

Figure 2.4 shows the irradiance of Equation (2.6) at a distance $R = 50m$, with the divergence angles $\theta_{FWHM_x} = 0.02\,\text{deg}$ and $\theta_{FWHM_y} = 0.2\,\text{deg}$.

Note that $I(x, y)$ is normalized to unity in the simulation as stated with Equation (2.2) in order to keep a constant total power independently of the target range.

2.2.2 Temporal Distribution: Pulse Shape

The time propagation of the laser signal is modelled as pulses. Two models found in the literature have been selected to be used in the LADAR simulation. In the

first one, the laser pulse travels with a time propagation which has been modelled in [7] as:

$$p(t) = (t/\tau)^2 \cdot \exp(-\frac{t}{\tau})$$
$$\tau = \frac{T_{1/2}}{3.5} \tag{2.8}$$

where $T_{1/2}$ is the Full Width at Half Maximum (FWHM) of the pulse.

Assuming that one works with a constant signal power:

- if $T_{1/2}$ is decreased, the pulse becomes narrower and will look like a peak. This peak is detected and may be interpreted as noise by the receiver which fails in detecting this pulse.

- if $T_{1/2}$ is increased the pulse will be flatter and may not reach the detection ceiling. The receiver fails in detecting this pulse.

A compromise has to be found and the designer engineer can discover different properties of the laser pulse changing $T_{1/2}$. This model is the most accurate one and is used in [1, 2, 7, 8]. A plot of Equation (2.8) is shown in Figure 2.5 (plain line curve).
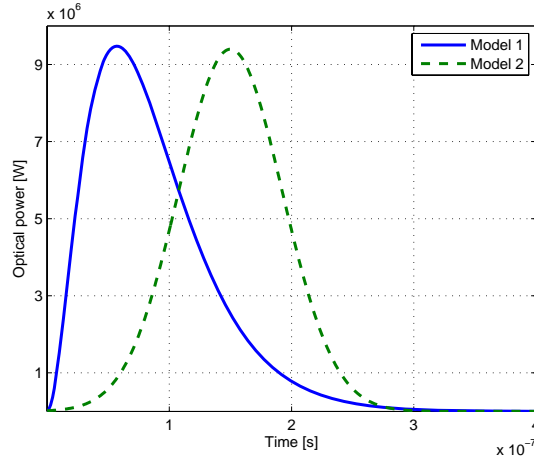
Figure 2.5. Normalized laser pulses with $T_{1/2} = 100$ ns.

The second model, more basic, is called Gaussian pulse and comes from [9]. It describes pulses with a temporal profile which has a Gaussian shape as follow:

$$p(t) = \exp\left[-4\log(2) \times \left(\frac{t - 3/2 \times T_{1/2}}{T_{1/2}}\right)^2\right], \tag{2.9}$$

where $T_{1/2}$ has the same meaning as in Equation (2.8). A realization of Equation (2.9) is shown in Figure 2.5 (dashed line curve).

Note that $p(t)$ is normalized to unity in the simulation as stated with Equation (2.2) in order to keep a constant total power independently of the pulse shape.

2.3 Propagation: Atmospheric Effects

The atmospheric effects limit the performances of laser systems since the laser pulse travels through the air. Many complex phenomena as turbulences, beam broadening or intensity variations occur and perturb the laser beam. If the reader is interested in finding more details about atmospheric propagation, it can be found in [2, 7, 10, 11]. The weather is not a parameter that can be controlled and therefore is not part of the scope of this work. Consequently, the atmospheric effects in the LADAR simulation are reduced to the aerosol attenuation only. The gases and particles in the air absorb and reflect the laser light. This creates a loss modelled by Beer's law which represents the attenuation of the beam power with the travelled distance. Assuming a constant atmospheric extinction coefficient, the law reduces to a familiar form:

$$T_a = \exp(-\alpha z), \tag{2.10}$$

where

T_a : one-way attenuation factor,
α : atmospheric extinction coefficient in (m^{-1}),
z : range dimension.

Since the laser pulse travels twice the distance to the target before reaching the receiver, it is affected by $T_a \times T_a = T_a^2$. The Figure 2.6 shows a plot of the squared attenuation factor.

2.4 Target Interactions

The interactions between the laser beam and the surface of the target result from complicated processes hard to model. It depends on two main characteristics of the surface: its slope and its microscopic properties. For detailed discussions about target interaction and reflection, the reader will refer himself to [1, 7, 12]. In the following, the target modelling done in the LADAR simulation is explained and followed with the description of the target reflection process.

2.4.1 Target Modelling

As it has been shown previously, the range from the laser source to the target plays a preponderant role in the LADAR simulation. For this reason, the target has to be modelled in terms of distance. The LADAR system is on board a platform.

This platform is flying at a constant altitude, following a straight trajectory and with a constant forward-looking angle. The dimensions of the target to be scanned being much smaller than the flight altitude, the assumption is that the scenery can be considered as seen from a fixed point of view. That is to say that the scenery's distortion due to the platform's motion is not taken into account. It yields that the 3D description of the scenery, containing the target, can be modelled by a 2 dimensional picture while working with a fixed forward-looking angle. This 2D picture is adapted in function of the angle of view, that is to say it is changed when the forward-looking angle is modified.

After having frozen the 3D scenery description into a 2D picture according to the forward-looking angle, the LADAR simulation needs the distance to each point of the 2D picture. Here appears the concept of *range image*: each pixel contained in the image has the value of the distance to an arbitrary origin (the expressions: "distance image" or "range template" are also used in the literature). In the LADAR simulation, this origin is the laser source. Thus, the pixels values represent the range to the laser source. Figure 2.7 is an example of range image in which the brightness decreases with the range. The generation of the range images is done via an external program. It is based on a 3D description of the target from which one can specify the visualization parameters (orientation, distance, resolution...). Thus, the program displays the range image with respect to the distance to the camera which, in our case, is equivalent to the laser source.

2.4.2   Target Reflection

As stated before, the reflection of the laser beam on a surface depends on the slope and the microscopic properties of the surface. This affects the amount of electro-magnetic radiation reflected as well as the directions in which the light is reflected. In a primary approach, these phenomena are not taken into account. A *constant*
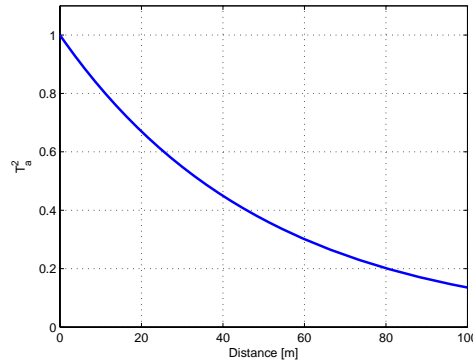
Figure 2.6. Squared attenuation factor, T_a^2, with $\alpha = 0.01$.
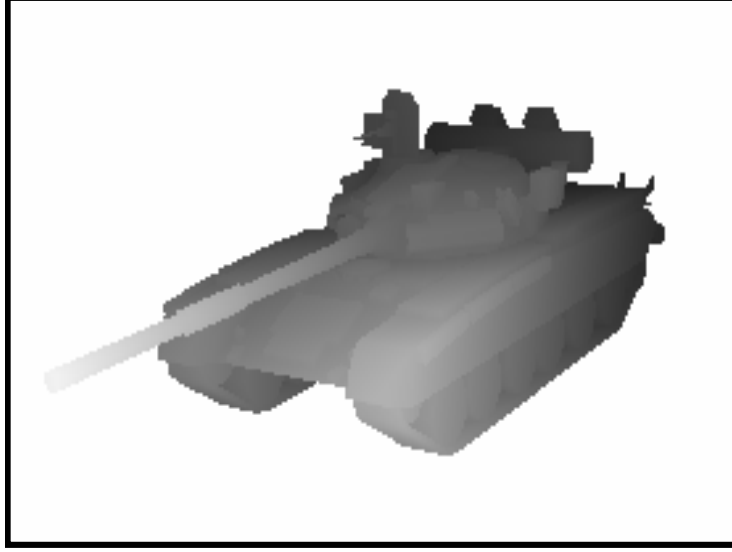
Figure 2.7. Range image of a tank T80.

term ρ, notably independent of the incidence angle, is used and represents the total hemispherical target reflectance. It is the percentage of re-emitted electromagnetic power in the reflection. As an example, a white surface will have a bigger ρ than a black surface since the white surface re-emits more light.

In Section 2.6, in which the LADAR range equation is derived, the terms *Lambertian* targets and *extended* targets are used. These are directly related to the Lambert's law which is best described here as done in [13]:

$$P_{reflected}(\theta) = P_0 \cdot \cos(\theta) \tag{2.11}$$

where $P_{reflected}(\theta)$ is the intensity of a small incremental area of the source in a direction at angle θ from the normal to the surface, and P_0 is the intensity of the incremental area in the direction of the normal. Equation (2.11) says that the total radiant power observed from a *Lambertian* surface is directly proportional to the cosine of the angle θ between the observer's line of sight and the surface normal. The law is also known as the *cosine emission law* and corresponds to the model used in the LADAR range equation derived in Section 2.6.

2.5 Receiver Characteristics

The receiver is an important stage in all the LADAR systems. It is characterized by the detection technique (direct or coherent), the area of the receiver element and the optical efficiency.

2.5.1   Detection Technique

The LADAR simulation uses the direct detection. The receiver consists in a photo-sensitive element which generates a signal directly proportional to the quantity of optical power received. This technique, contrary to the coherent detection, uses a conventional passive optical receiver. More details about detection techniques are found in [10].

2.5.2   System Efficiency and Sampling Frequency

The ability of the receiver to detect the incoming optical power is limited by the efficiency of each of its subcomponents. Since it is impossible to know which kind of design has been used to build the receiver, it is impossible to know every efficiency. A previous estimation of the total loss due to the receiver has to be carried out before including it in the LADAR simulation. The receiver efficiency appears as a simple coefficient (a percentage) that can be modified by to the user and called η_{syst}. It will limit the received power.

Another aspect which limits the performances of the LADAR system is the rate to acquire data used at the receiver. The signals at the receiver are sampled through an A/D (Analogic/Digital) converter at the sampling frequency F_s. This permits the reducing of the amount of data to be processed and thus reduces the computation time.

- High F_s provide better range resolutions in every pixel but increase the pixel processing time. As a consequence, the PRF (developed in 3.4) becomes lower: the final image has poor resolution but good precision in every pixel.

- Low F_s give bad range resolution but decrease the pixel processing time. As a consequence, the PRF (developed in 3.4) becomes higher: the final image has good resolution but poor precision in every pixel.

Consequently, a compromise has to be found between the cross-range dimension accuracies (resolution) and the range dimension accuracy (pixel precision). To be able to study this problem, the parameter F_s is included in the LADAR simulation. However, the computation time depends much on the algorithms and hardware used at the processing stage. Therefore, this is hard to predict and only F_s appears in the simulation allowing to experience different range precisions.

2.5.3   Noises & Noise

As in all conventional optical systems, the LADAR receiver is subject to several noise sources: ambient backgrounds, detector dark current, thermal noise and quantum shot noise. Once again most of these perturbations are closely related to the construction of the receiver, which is unknown. More than 15 parameters have to be estimated to be able to simulate the noises. Consequently, in order to provide a

more schematic model, a global factor handles the noise. Indeed, if all these noises are unknown, it is known that their combination yields a Gaussian distribution. Moreover, the standard deviation of this Gaussian distribution has the value of the Noise Equivalent Power (NEP). Since the power of the sent pulse is known, it is possible to modify the Signal to Noise Ratio of the received signal. In the LADAR simulation, the SNR can be modified and then reproduce different noise levels.

An important parameter for minimizing the noise at the receiver is the bandwidth B of the electronics following the optical receiver. With a too large bandwidth, too much noise is admitted in the system. With a too narrow bandwidth, parts of the received signal are modified or suppressed. To increase the SNR, a compromise has to be found between accepting noise and modifying the received signal. The shape of the sent pulse is known so this implies that its frequency contents are also known. Under the assumption that the received signal is not too distorted during its travels and during the reflection, one can consider that the sent pulse and the received pulse are similar (in time and frequency domains). This assumption is realistic for a long pulse, which is the case in the LADAR simulation since the pulse width lies around 100 ns. Then the compromise on B is done by looking at the spectral content of the sent pulse which defines the required bandwidth B.

2.6 LADAR Range Equation

To conclude these previous sections about laser theory, the LADAR range equation used in the LADAR simulation is derived and can be found in [5]. It permits to compute the total optical power incident on the receiver element. The LADAR using electromagnetic propagation, the microwave radar range equation, as found in [14], applies:

$$P_r = \frac{P_t}{\Omega_s} \times \frac{\sigma}{4\pi R^2} \times \frac{\pi D^2}{4} \times T_a^2 \times \eta_{syst} \tag{2.12}$$

where
P_r : received signal power (W),
P_t : transmitter power (W),
Ω_s : scattering steradian solid angle of source,
σ : effective target cross section (m^2),
R : target range (m),
D : receiver aperture diameter (m),
T_a : attenuation factor,
η_{syst} : system efficiency.

The effective target cross section is defined in [14] as:

$$\sigma = \frac{4\pi}{\Omega_t} \cdot \rho \cdot dA \tag{2.13}$$

where

Ω_t : scattering steradian solid angle of target,
ρ : target reflectance,
dA : target area (m^2).

For *Lambertian* targets (diffuse targets), Ω_t tends to be replaced by the value associated with the standard scattering diffuse target having a solid angle of π steradians.

In the LADAR simulation, the footprint is much smaller than the dimensions of the target. Thus, the target intercepts totally the laser beam and it is classified as an *extended target*. In that case, dA corresponds to the area illuminated by the laser beam on the target. Moreover, one can approximate the solid angle Ω_s by a flat surface since the laser footprint has small dimensions. That is to say the z dimension is neglected, only the extensions along the x and y cross-range dimensions are considered. Thus, the flat surface corresponds to the laser footprint on the target: $dA = \Omega_s$. This assumption is valid because the divergence angles and the target range are small which gives to a small footprint area, typically $< 0.1\ m^2$. Finally, under the previous approximations and substituting Equation (2.13) in Equation (2.12) lead to the *LADAR range equation*:

$$P_r = \frac{P_t \rho D^2}{4R^2} \times T_a^2 \times \eta_{syst} \qquad (2.14)$$

where all terms are as previously defined.

The initial microwave radar range equation reduces into a simpler form, Equation (2.14), that the reader can find in [4, 5, 7]. It provides good insight on what happens with the optical power, P_t, during its propagation. T_a^2 is the two-way attenuation factor caused by the particles and gases present in the atmosphere. ρ represents the proportion of power reflected by the target and η_{syst} the efficiency of the system. D characterizes the aerial extension of the receiver which collects the reflected power. Equation (2.14) also shows the typical dependence, for *extended* targets, of the received power with the inverse square of the range.

Part II

The Simulation Software

Chapter 3

Simulation

The LADAR simulation has been developed to support future LADAR hardware device development and to support system engineering studies. The key attributes of this LADAR simulation are that i) it is modular, allowing great variations in design parameters, such as pulse shapes, power, sampling frequency, flight characteristics or signal processing; ii) it works with arbitrary targets through the use of the appropriate 2D range image describing the scenery; iii) the models used are simple, which give understandable parameters for the user.

3.1 Discretization

Lets start by recalling the description of the laser beam intensity $U(x, y, t)$ of Equation (2.2) page 6:

$$U(x, y, t) = I_0 \cdot p(t) \times I(x, y)$$

where x, y and t take on discrete values.

This brings up the question of the resolution choices both in temporal and spatial domains. Those resolutions have to be adapted to the characteristic dimensions (geometrical and temporal) in the simulation, typically:

- a pulse has a width of 100 ns.

- a footprint has an area of $0.2 \times 0.2\ m^2$ for a target at 50 m.

The first consequence is that the *temporal resolution* has been fixed to 1 ns with respect to the pulse width. The reason for this choice is that it gives a pulse described by one point every ns, that is to say a discretization done at a frequency of $10^9\ Hz$. As a consequence, all the signal sampled at this frequency can be considered as continuous signals since the sampling done at the receiver stage uses a frequency $\propto 10^7 - 10^8\ Hz$. On the other hand, the spatial resolution depends on the footprint size which may change in the simulation. Actually the user can set up the number of subareas constituting the footprint (see paragraph entitled -OPTIONS- in

Section 4.1.1), the direct consequence being a resolution change. Nevertheless, with the default parameters, the *spatial resolution* is $1 \times 1 \ cm^2$. Generally speaking, the resolutions have been chosen according to the computer power available nowadays and to generate time efficient results with good accuracy.

3.2   Overview and Modules Description

The reader is reminded here of the process decomposition found in Figure 2.1 page 5 in order to have a clear view of the principle. It is a good schema to review before reading the explanations of the different LADAR simulation modules.

The simulation program is entirely written in Matlab. It consists of several modules passing data from one to the next by variables. Two kinds of variables are found in the program i) the *global variables* correspond to the parameters set up by the user or fixed values which will not change during the execution; ii) the *intern variables* subject to modifications are passed through the input/output arguments of the different modules. Figure 3.1 presents these main modules associated to their principal parameters and concepts. They are organized in the logical order in which they appear in the simulation program.

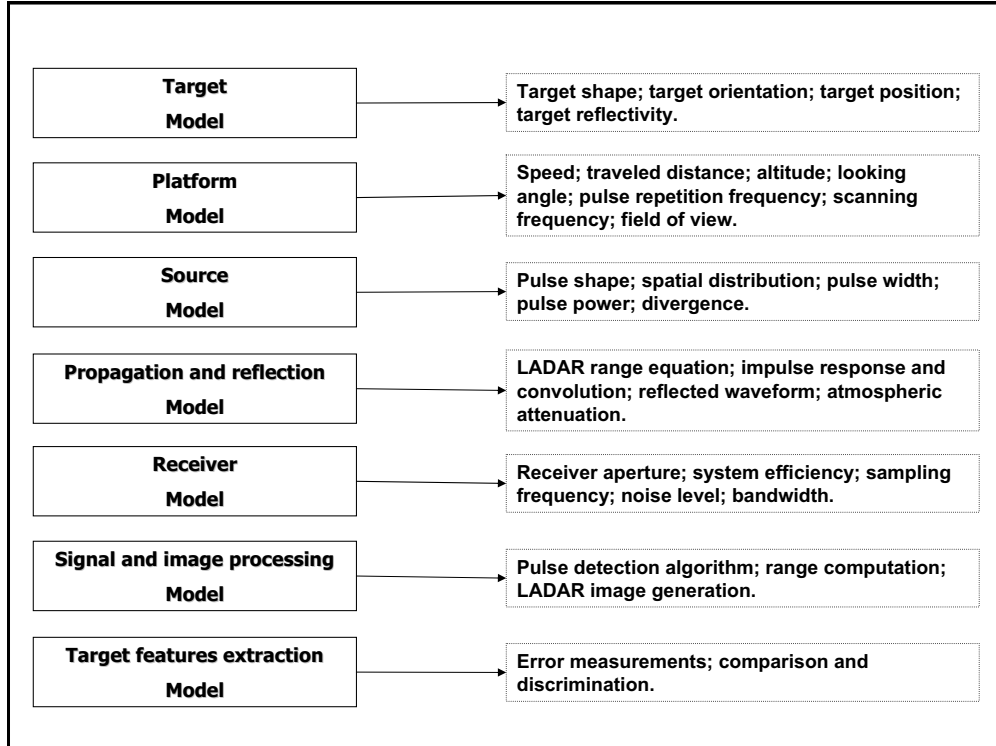| Target Model | → | Target shape; target orientation; target position; target reflectivity. |
Platform Model	→	Speed; traveled distance; altitude; looking angle; pulse repetition frequency; scanning frequency; field of view.
Source Model	→	Pulse shape; spatial distribution; pulse width; pulse power; divergence.
Propagation and reflection Model	→	LADAR range equation; impulse response and convolution; reflected waveform; atmospheric attenuation.
Receiver Model	→	Receiver aperture; system efficiency; sampling frequency; noise level; bandwidth.
Signal and image processing Model	→	Pulse detection algorithm; range computation; LADAR image generation.
Target features extraction Model	→	Error measurements; comparison and discrimination.

Figure 3.1. Main simulation processing modules.

Nevertheless, it is also interesting to see the repartition of the modules related to the process decomposition as shown in Figure 3.2. The laser on board a platform is described by the **platform model** and the **source model**. The propagation in the atmosphere has been merged with the reflection since it is only an attenuation coefficient which does not required a full module. The target interactions are handled by **the propagation and reflection model** and the **target model**. Finally, the receiver stage consists of the **receiver model**, the **signal and image processing model** and the **target features extraction model**.
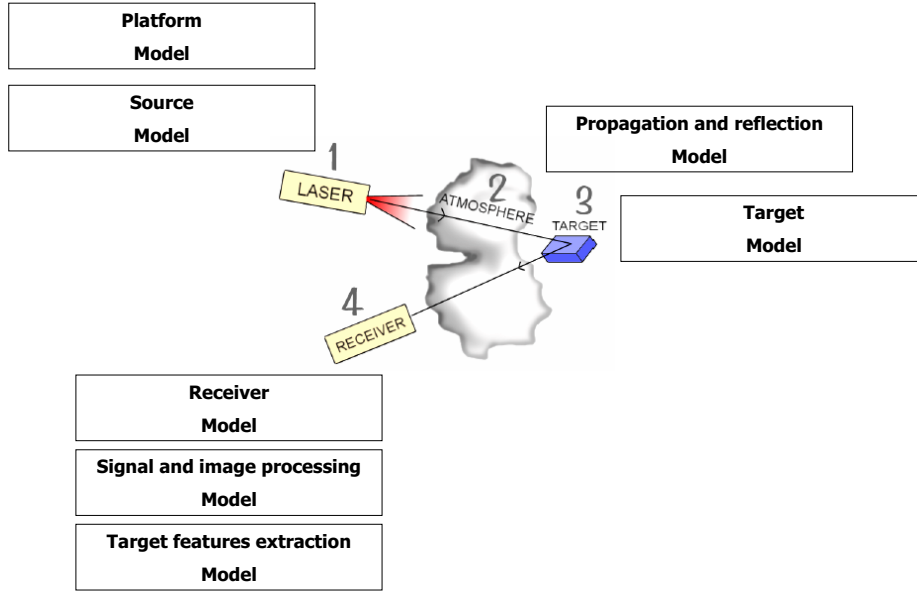
Figure 3.2. Modules repartition.

3.3 Simulation Steps: Procedure

The key of success in the LADAR simulation is the decomposition of the laser beam in time and space. The components disassembly presented in Equation (2.2) page 6 has been derived from [3, 4, 7]. It represents the core of the simulation program. The main idea is that one laser shot provides one pixel of the final LADAR image. The pixel has same resolution as the size of the laser footprint and is obtained using one single pulse. The simulation steps are presented in the following and stand for the tremendous amount of lines of code. Figure 3.3 gives a schematic view of the principles used.

1. Define all the parameters required for the simulation concerning the: platform, laser source, atmosphere, target, noise level and receiver.

2. For every laser shot, create the laser pulse in time and create the laser footprint in space[1] about to illuminate the pixels on the 2D range image:

   $p(t)$: laser pulse shape in time.

   $I_t(x, y)$: laser footprint on the target (irradiance at target range).

3. Match the resolution of the 2D range image describing the target with the grid corresponding to the laser beam profile in the spatial domain ($\Leftrightarrow$ the footprint). Indeed, as stated in Section 2.2 and developed in Section 3.1, the laser beam profile is decomposed in its cross-range dimensions (x,y). Each cross-range component, or *subarea*, corresponds to the energy contained in a square (typically $1 \times 1\ cm^2$ at target range). The user can choose the number of subareas within the laser footprint. The size of the subareas depends on their quantity, the target range and the beam divergence. Consequently, it is necessary to adapt the resolution of the 2D range image to the subareas decomposition for the next steps of the simulation.
   At the end of this step, each subarea of the footprint has the same dimensions as the pixels of the 2D range image describing the target.

4. Consider one pixel P_p. In order to compute the waveform of the reflected pulse, one needs first the *impulse response* h_p of P_p. Then, send one Dirac $\delta(t)$ (one sample of amplitude one) on P_p and apply the LADAR range equation in each subarea contained within this pixel. The latter meaning: compute the reflected power from each subarea reaching the receiver. For every subarea, a value $P_{i,subk}^{received}$ is obtained where i is the round trip time with respect to the subarea k. The slope is not a parameter taken into account during the reflection: each cross-range component is treated as if it encounters a subarea that is perpendicular to the line of sight to the sensor. However, a pulse ($\Leftrightarrow I_t(x, y)$) may see non perpendicular surfaces as a set of subareas at different ranges.

5. Sum the reflected powers $P_{i,subk}^{received}$ with the same time indices i. It results a temporal signal which is the *impulse response* h_p of the considered pixel P_p.

$$h_p(i) = \sum_{subk,i=i} P_{i,subk}^{received}$$

$h_p(i)$: impulse response of P_p.

---

[1]see appendix B for the creation of the source diode model. It contains the m-file including an example.

6. Convolve the *impulse response* h_p with the temporal laser pulse $p(t)$ to form the reflected power detected by the receiver. This corresponds to the total received power for the considered pixel P_p.

$$P_{P_p}^{received}(t) = h_p(t) * I_0 p(t)$$
$$= I_0 \cdot \int_{-\infty}^{+\infty} h_p(\tau) \times p(t - \tau) \cdot d\tau$$

where

$P_{P_p}^{received}(t)$: total received power from P_p,

I_0 : laser pulse power.

Note that according to Section 2.5.3 page 14: $P_{P_p}^{received}(t) \equiv k \times p(t)$, for all $k \in \mathbb{R}$.

7. Let the Gaussian noise disturb the total received power according to the SNR set up by the user. The signal $x(t)$ obtained is used in the pulse detection.

$$x(t) = P_{P_p}^{received}(t) + n(t)$$

$n(t)$: additive Gaussian noise with a standard deviation $\sigma = $ NEP.

$x(t)$: noisy reflected pulse from P_p.

8. A pulse detection algorithm determines, from the signal $x(t)$, the round trip time of the pulse reflected by the pixel P_p, (see Section 3.5 page 28 for the details about the pulse detection algorithms).

9. The latter permits to compute the distance d_p to the pixel P_p using Equation (2.1). The value d_p is assigned to the corresponding pixel on the final LADAR image (all the subareas constituting the original footprint are merged onto one unique final pixel P_p at distance d_p).

3.4   Airborne Laser Scanning

The detector is made of one receiver cell. This implies that one pixel of the final LADAR image is obtained for each laser shot. Consequently, the scenery needs to be scanned by the laser beam in order to build, pixel after pixel, the LADAR image. The following presents the basic formulas concerning airborne laser scanning in order to understand some basic principles used in the LADAR simulation. The reader will find more detailed descriptions in [15, 16]. The scan method chosen produces a Z-shaped scan as presented in Figure 3.4.

There are four main parameters influencing the performances of a Z-shaped scan:
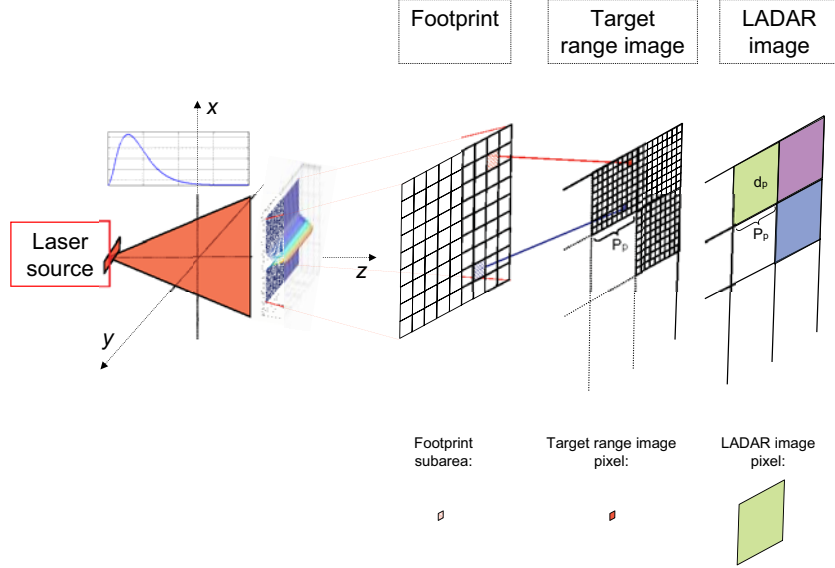
Figure 3.3. Simulation principle.

PRF : the Pulse Repetition Frequency (how often a pulse is sent),
F_{sc} : the scan frequency (to go from left to right swath border, or the opposite),
V : the velocity of the platform,
S : the swath width.

3.4.1   Footprint

Before all, lets start by giving the formulas related to the laser footprint. All the notations and symbols are reported in Figure 3.4 and Figure 3.5.

The two cross-range dimensions of the laser footprint are given by:

$$l_x = 2R \cdot \tan\left(\frac{\theta_{fwhm,x}}{2}\right)$$

$$l_y = 2R \cdot \tan\left(\frac{\theta_{fwhm,y}}{2}\right)$$

$$\text{with } R = \frac{h}{\sin\delta}$$

where
l_x, l_y : footprint cross-range dimensions,
$\theta_{fwhm,x}, \theta_{fwhm,y}$: divergence angles,

Figure 3.4. Z-shaped laser scan.

Figure 3.5. Laser footprint.

R : target range,
h : flight altitude,
δ : forward-looking angle.

To make things handier in the image generation, it is better to handle pixels with a square shape. Since l_x and l_y are different, the resulting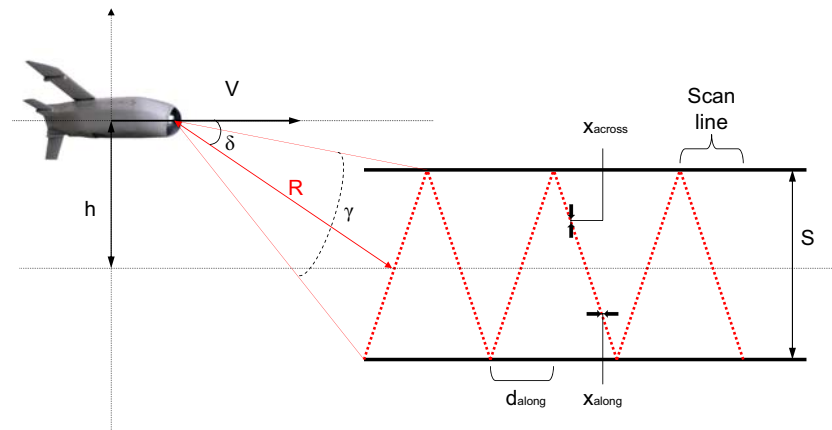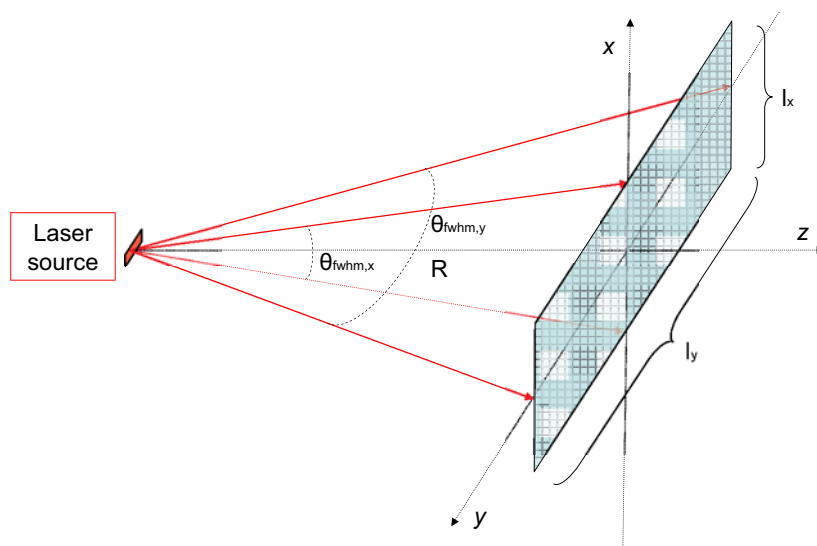 footprint is rectangle as seen in Figure 3.5. To tackle this problem the value l, defined as the maximum of l_x and l_y, is used to create a square footprint.

$$l = \max(l_x, l_y)$$

Taking the longest dimension prevents from truncating too drastically the beam profile. This results in a beam profile similar to the one shown in Figure 2.4 page 9. The two flat parts surrounding the beam profile are neglected in the computations in order to save time.

Moreover, an extra constraint is added on the divergence angles $\theta_{fwhm,x}$ and $\theta_{fwhm,y}$ of the source diode model described in Section 2.2.1. They cannot be chosen freely and are linked by the relation:

$$\theta_{fwhm,x} = \frac{1}{10} \times \theta_{fwhm,y} \tag{3.1}$$

Equation (3.1) shows the direct influence of $\theta_{fwhm,y}$ on $\theta_{fwhm,x}$. In the LADAR simulation, the user can variate $\theta_{fwhm,y}$ which corresponds to variating the longest dimension of the footprint, that is to say l.

Finally, the unique characteristic dimension of the footprint is reduced to:

$$l = 2R \cdot \tan\left(\frac{\theta_{fwhm,y}}{2}\right)$$
$$l \approx R \times \theta_{fwhm,y} \tag{3.2}$$

where all the terms are as previously defined.

Since the divergence angles $\theta_{fwhm,i}$ are small ($\ll 0.5$ deg), the approximation in Equation (3.2) is valid. It shows the direct proportional relation between the target range, R, and the footprint dimension l. Doubling the distance R (or the flight height h) will increase the footprint area by a factor 4.

3.4.2   Swath Width

The following equations, based on Figure 3.4, give the swath width as a function of the altitude and the field of view:

$$S = 2R \cdot \tan\left(\frac{\gamma}{2}\right)$$
$$S \approx R \times \gamma$$
$$S \approx \frac{h}{\sin\delta} \times \gamma \tag{3.3}$$

where
  S : swath width,
  γ : LADAR's field of view,
  all the other terms are as previously defined.

Equation (3.3) reveals the linear relation between the height of flight h (as well as the target range R) and the swath width S. One sees that doubling the flight height, will also double the swath width.

3.4.3 Number of Points per Scan Line

While the laser beam scans from one side to the other, laser pulses are sent at a frequency PRF in order to create the pixels of the LADAR image. The number of points per scan line is given by:

$$N = \frac{PRF}{F_{sc}} \tag{3.4}$$

where
  N : number of points per scan line,
  PRF : Pulse Repetition Frequency,
  F_{sc} : scan frequency.

Note, in Equation (3.4), the independence of N regarding the flight height h (and the target range R) as well as the swath width S.

3.4.4 Point Spacing

The formulas related to the point spacing are given in the following. They are closely related to the LADAR image resolution.

Point spacing along the track. The distance between the two extreme points on the same line of scan (see d_{along} in Figure 3.4) is given by:

$$d_{along} = \frac{V}{F_{sc}} \tag{3.5}$$

where
  d_{along} : see Figure 3.4,

F_{sc} : scan frequency,
V : velocity of the platform.

Its yields the range point spacing:

$$x_{along} = \frac{d_{along}}{N} \tag{3.6}$$

where x_{along} is the distance between two points in the range direction, (see x_{along} in Figure 3.4).

Point spacing across the track. Using the swath width S derived in Section 3.4.2, it yields:

$$x_{across} = \frac{S}{N} \tag{3.7}$$

where x_{across} is the distance between two points in the direction orthogonal to the range direction, (see x_{across} in Figure 3.4).

3.5 Signal Processing and Pulse Detection

In theory, the idea of computing the range to an object by measuring the time of flight of a pulse is an efficient method. Nevertheless, in reality, it depends much on how the measurements are done and thus on how the pulse is detected. In the LADAR simulation the user can choose between three methods. The first two are based on a direct use of the temporal shape of the received waveform. The last one uses a filtering method.

3.5.1 CFD

CFD stands for *Constant Fraction Discrimination*[2]. It is a cost-efficient algorithm which permits to detect a noisy pulse with good accuracy. The following description is directly taken from the well documented book [10] and is related to the Figure 3.6 taken from [10].

> "CFD is accomplished by splitting the incoming signal into two channels, delaying one channel by one half of a pulse width, and subtracting the delayed channel from the original. This results in a positive and then negative signal with a characteristic S-shaped profile. It has been shown that the zero crossing of this derived signal is very insensitive to amplitude fluctuations. It is, however, somewhat sensitive to pulse length variations."

---

[2]the m-file (including an example) related to the CFD algorithms is found in the appendix C.

The zero crossing of the S-shaped profile seen in Figure 3.7 is used to trig a timer. The CFD algorithm is applied to the sent pulse to start the clock and then applied to the received pulse to stop the clock. This provides a time directly used in the range computation.

3.5.2 CFD 50%

The principle of the *CFD 50%* method is based on the idea of the 50% leading edge detection. The latter consists in taking the reference time at a time where the leading edge of the pulse reaches 50% of the pulse's maximum. In some cases, it permits to detect more details than with a basic method based on the detection of the pulse maximum, as demonstrated in [1]. So does the CFD 50% method as illustrated in Figure 3.7: to the zero crossing of the S-shaped profile corresponds a value on the pulse, y_0 (note that it is not the maximum); the reference time is then taken when the leading edge of the pulse reaches 50% of y_0. Empirically, the CFD 50% method gives substantially better results than the CFD method.

3.5.3 Matched Filter

The *matched filter* principle is used extensively in pattern recognition and signal detection. It is the optimal linear filter for maximizing the signal to noise ratio (SNR) in the presence of additive stochastic noise, n.

Given a transmitter pulse shape $p(t)$ of duration T, the *impulse response, h_{opt}, of the matched filter* is given by:

$$h_{opt}(t) = k \times p(T - t) \qquad , \text{for all } k \in \mathbb{R}. \tag{3.8}$$

Equation (3.8) shows that the duration and the shape of the impulse response of the optimal filter is determined by the pulse shape $p(t)$. $h_{opt}(t)$ is a scaled, time-reversed and shifted version of $p(t)$.
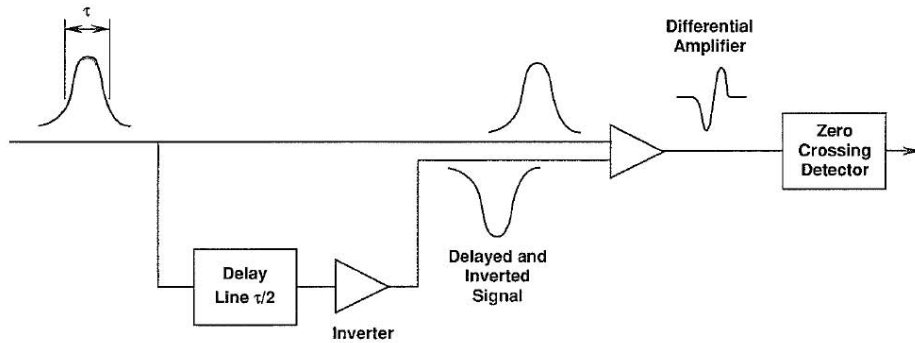

Figure 3.6. CFD peak detection.
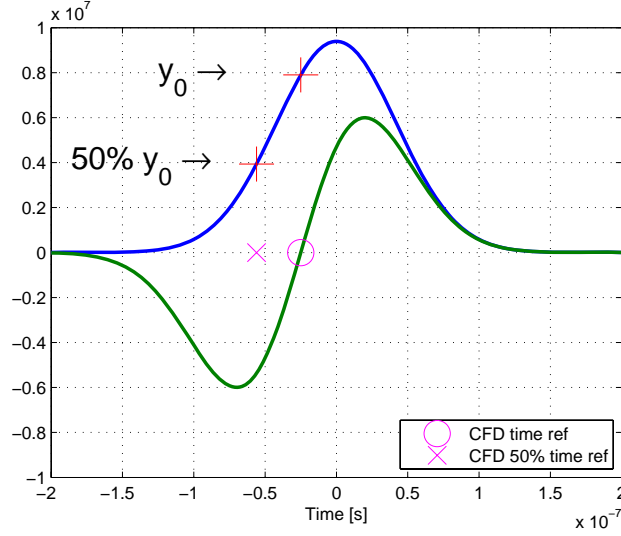
Figure 3.7. CFD and CFD 50%.

This is applied in the LADAR simulation, in which a pulse p is sent out and one wants to find something, in the noisy reflected signal x, similar to what was sent out. The schema of the matched filtering is presented in Figure 3.8.
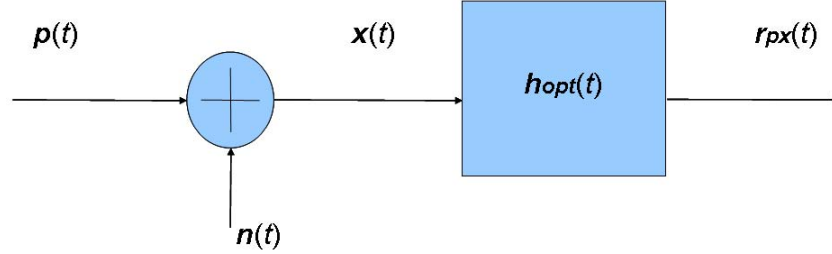
Figure 3.8. Matched filter.

The matched filter is obtained by correlating a known signal p, or template, with the unknown signal x to detect the presence of the template in the unknown signal. This is equivalent to convolve the unknown signal with a time-reversed version of the template, as shown in Equation (3.8). By time reversing p, the convolution implemented by filtering is transformed into a sliding cross-correlation operation between the input signal x and the sought signal p leading to $\hat{r}_{px}$, see Figure 3.8. The occurrences of p in x are detected in each peak of $\hat{r}_{px}$. Detailed plots of the filtering process are found in Section 4. For each occurrence corresponds a time used to trig a timer and then compute the round trip time of the pulse.

Chapter 4

Graphical User Interface

The Graphical User Interface (GUI) is the link between the user and the code. This gives an efficient way of working without interacting directly on the simulation program. Knowing that one picture says more than one thousand words, the GUI's efficiency comes from i) it is simple to use despite the comfortable level of abstraction of the simulation; ii) it is interactive thanks to the numerous plots displayed at every parameter change or simulation runs done by the user; iii) the user has a constant overview of all the parameters used.
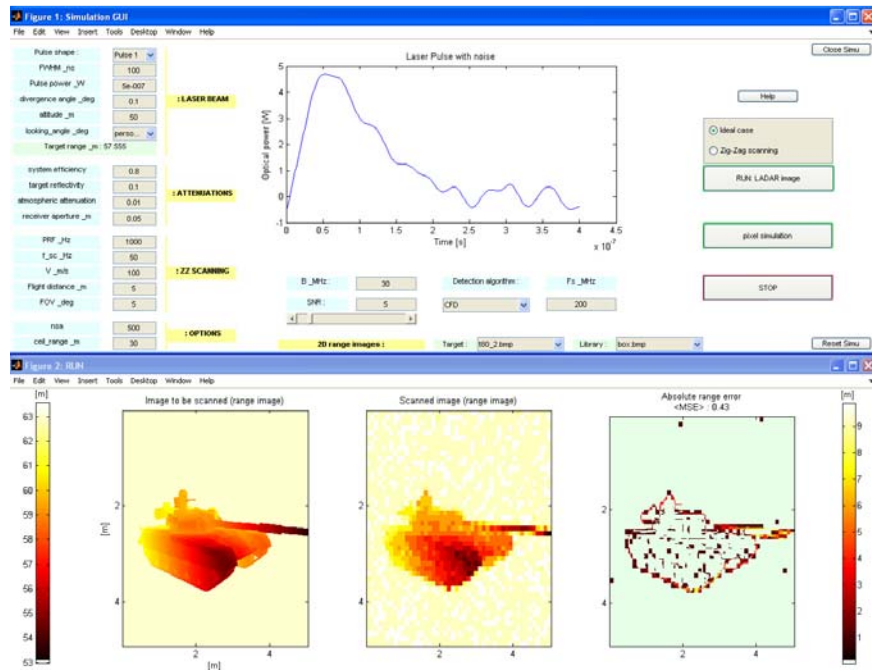

Figure 4.1. Screenshot LADAR GUI.

4.1   Front Panel

The front panel[1] is the window located in the top half of the computer's screen after running the simulation file (see figures 4.1 and 4.2 for details). It consists of several types of elements which are best described here:

- *axes* : axes enable the GUI to display graphics, such as graphs and images.

- *text* : static text boxes display lines of text. Static text is typically used to label other controls, provide directions to the user, or indicate values.

- *edit* : editable text fields enable users to enter or modify parameters values. Each new value must be validated by pressing enter.

- *pop-up menu* : pop-up menus open to display a list of choices when pressed. When not open, a pop-up menu indicates the current choice.

- *push button* : push buttons generate an action when pressed. To activate a push button, click the mouse button on the push button.

- *slider* : sliders accept numeric input within a specific range by enabling the user to move a sliding bar. The user move the bar by pressing the mouse button and dragging the pointer over the bar, or by clicking in the trough or on an arrow. The location of the bar indicates a numeric value, which is selected by releasing the mouse button.

- *radio button* : radio buttons are useful when providing the user with a number of independent choices. They are mutually exclusive within a group of related radio buttons (i.e., only one is in a pressed state at any given time). To activate a radio button, click the mouse button on the object. The state of the device is indicated on the display.

4.1.1   Front Panel: Left Columns

The left side of the front panel gathers simulation parameters as seen in Figure 4.2. Every line is made up of one *text* element giving the name of the parameter that can be modified editing the *edit* element. To be precise, there are three exceptions to that format. The 1st line permits to change the pulse shape using a *pop-up menu* instead of an *edit* element. Line 6 corresponds to the forward-looking angle which can be modified only by choosing predefined values. These values are stored in the corresponding *pop-up menu* instead of an *edit* element. Line 7 is only a *text* element standing for an indicator of the distance to the target. The value is actualized in function of the user's choices. As one notes in the Figure 4.2, the parameters are gathered within four distinct sections detailed in the following.

---

[1]a description of all the parameters contained in the front panel is found in the appendix A.
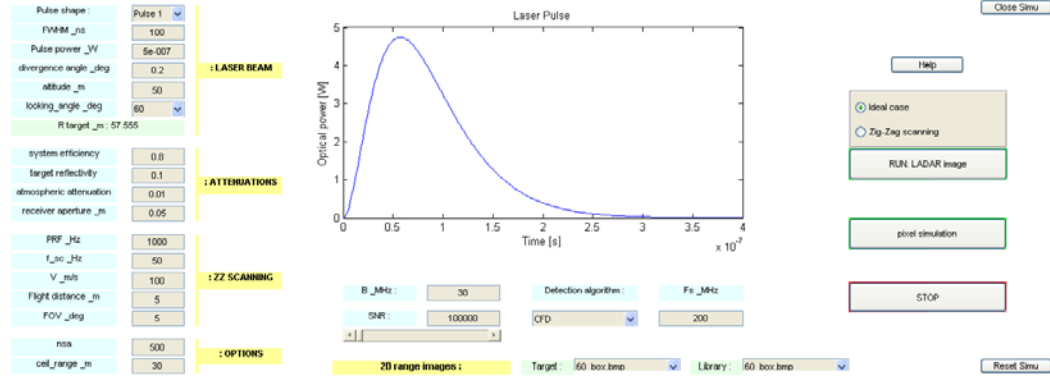
Figure 4.2. Front panel.

-Laser Beam-

It contains $6 + 1$ elements related to the laser pulse source model. These elements are: the pulse shape (*pulse shape*), the full width at half the maximum of the pulse (*FWHM*), the pulse power (*pulse power*), one of the two divergence angle seen in Section 3.4.1 (*divergence angle*), the altitude at which the platform is flying (*altitude*) and the forward-looking angle of the laser beam (*looking angle*). The last one is an indicator displaying the distance from the laser source to the target (*R target*).

-Attenuations-

This group gathers 4 parameters which have a direct influence on the received power: the *system efficiency*, the *target reflectivity*, the *atmospheric attenuation* and the *receiver aperture*. Their influence can be interpreted as a scaling in amplitude of the received signal.

-ZZ Scanning-

This part is related to the Zig-Zag scanning simulation case. These parameters are dedicated to this simulation case and describe the flight and scanning characteristics. They are: the pulse repetition frequency (*PRF*), the scan frequency (f_{sc}), the speed of the platform (*V*), the distance covered during the flight (*Flight distance*) and the field of view of the scanner (*FOV*).

-Options-

The 1st line allows to choose the number of subareas within the footprint (*nsa*) as stated in Section 3.1 (more subareas give better precision but required a longer computational time). The 2nd, and last line of the column, disables the detection of

objects located in between the laser source and a distance set up in the *edit* element (*ceil range*).

4.1.2 Front Panel: Central Elements

In the centre of the front panel seen in Figure 4.2, axes are used to display graphs and images. When it is useful, a graphic is displayed illustrating the effects of the new set up parameter. Every time that the user changes and validates a value, a graph is displayed within these axes. For example, it could be the new target image, the profile of the laser beam or the sampled signal.

Under the axes, there are the 4 parameters related to the receiver. Firstly, the receiver's bandwidth can be modified with the *edit* element entitled B. Secondly, the signal to noise ratio at the receiver can be changed in two ways: directly by typing a value in the *edit* element named SNR or using the slider (its value is then displayed in the *edit* element). Furthermore, the detection algorithm used in the signal processing can be selected thanks to the *pop-up menu* made of three items: *CFD*, *CFD 50%* and *matched filtering*. Finally, the sampling frequency is set up in the *edit* element named F_s.

The bottom line entitled *2D range images* displays the lists of the images available to be used as target and the images of the library. The content of these two lists is set according to the set up looking angle. The field *target* contains the image to be scanned in the simulation and the field *library* is the image used to do a comparison with the LADAR image of the target (see Section 4.3 to find details on the comparison done).

4.1.3 Front Panel: Right Side

On the right side of the front panel, one finds 6 *push buttons* and a group of 2 *radio buttons*. The latter permits to select the simulation case to be simulated. From top to bottom: the *Close Simu* button closes the whole simulation; the *Help* button displays the help file with the descriptions of all simulation controls; the *RUN: LADAR image* runs the simulation case indicated by the active radio button; the *pixel simulation* button displays the plots related to one single laser shot ($\Leftrightarrow$ one pixel); the *STOP* button breaks the running simulation and finally the *Reset Simu* closes and re-opens the GUI with the default parameters values.

4.2 Visualization Panel

The visualization panel is the window located in the bottom half of the computer's screen after running the simulation file (see Figure 4.1). It shows the results of the simulations (LADAR image and pixel simulation) ran by the user.

4.2.1 Pixel Simulation

The pixel simulation does not generate images but signals plots. It corresponds to one single laser shot done to detect the distance of one surface element (pixel) located at target range. Once the pixel simulation has been run, an array of 4 graphs are displayed in the visualization panel. The first row always provides the same information, that is to say a graph with the plot of the laser pulse sent and a graph with three other plots related to the received signal (received pulse, noisy received pulse and sampled noisy received pulse), an example is given in Figure 4.3.
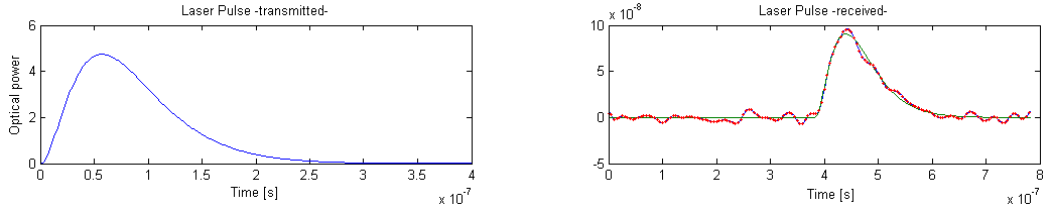
Figure 4.3. Pixel simulation: 1st row.

The 2nd row shows two graphs which depend on the detection algorithm selected: CFD algorithms or matched filter algorithm.

CFD Algorithms

To the *CFD algorithms* (CFD and CFD 50%) correspond the plots of the two significant curves of the method: the input pulse and the S-shaped profile with its zero crossing (see the algorithms descriptions in sections 3.5.1 and 3.5.2). Thus, the first plot contains these two curves for the sent pulse and the second plot as well but with respect to the sampled noisy received pulse, see Figure 4.4. Moreover, the red $+$ on the pulse corresponds to the triggering time ($\Leftrightarrow$ the zero crossing of the S-shaped profile) used for the range computation. On the other hand, the magenta $\times$ is the limit after which the detection is enable ($\Leftrightarrow$ the ceil range option described in Section 3.3).

Figure 4.4. Pixel simulation: 2nd row with CFD.

Matched Filter Algorithm

To the *matched filter algorithm* correspond the plot of the impulse response and the plot of the filter output (see the algorithm description in Section 3.5.3).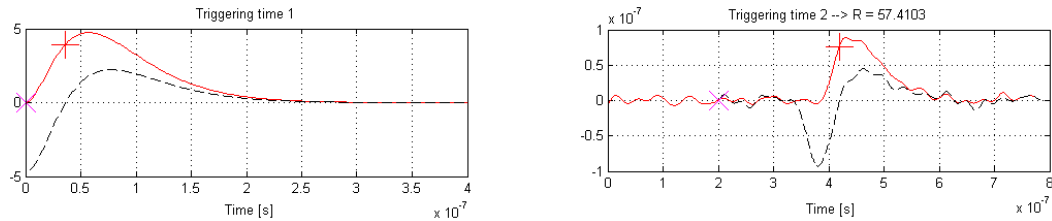 Moreover, the red + located at the maximum of the filter output ($\Leftrightarrow \hat{r}_{px}$ described in Section 3.5.3) stands for the round trip time of the pulse.
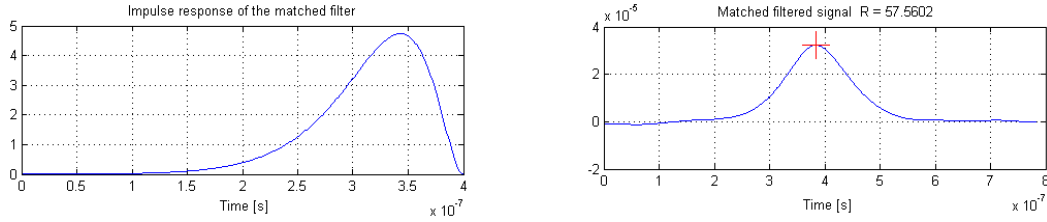

Figure 4.5. Pixel simulation: 2nd row with matched filter.

4.2.2   Simulation: LADAR Image Generation

In this second part describing the visualization panel, the LADAR image generation is presented. The range image of the target (selected in the *target* pop-up menu) is displayed on the first graph. The second graph shows the LADAR image generated through the simulation program. These two pictures are range images and the corresponding scale is located on the left side of the visualization panel. On the other hand, the third and last picture represents the absolute range error between the original target and the LADAR image. It reveals the error (see Section 4.3 for explanations on the error computations) between the two images and the related scale is located on its right side.

Ideal Case

The Figure 3.4 page 25 shows that in reality, the LADAR picture will be discontinuous because of the scan method. That is to say the resulting picture will contain pixels only along the Z-shaped pattern as seen in the central illustration of Figure 4.7. In the ideal case, this difficulty is skipped and continuous LADAR images are generated. This approximation can be interpreted as a LADAR system using a receiver made of one line of detector cells and flying at an appropriate speed. Consequently, all the footprints are joint and do not overlap. They cover *perfectly* all the original scenery. The resulting visualization panel, in the *ideal case*, is shown by Figure 4.6.
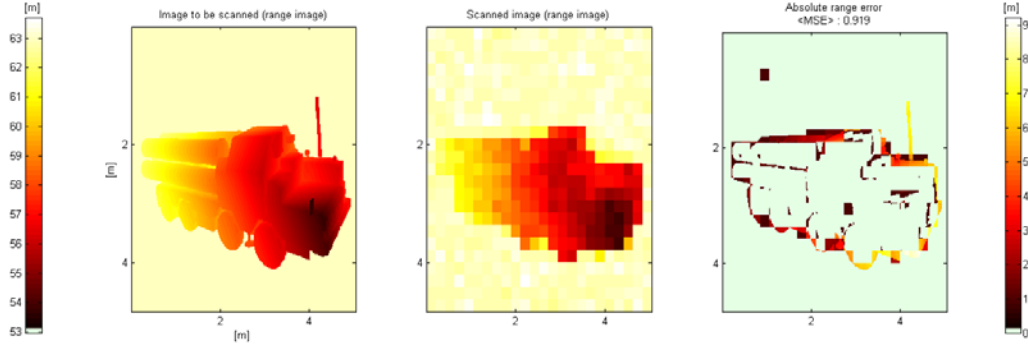
Figure 4.6. Simulation: ideal case.

Zig-Zag Scanning

The Zig-Zag scanning simulation is directly linked to the -ZZ SCANNING-parameters group of the front panel (Section 4.1.1). As shown in Section 3.4, the Z-shaped pattern depends simultaneously on several parameters (PRF, f_{sc}, V,...). It can happen that the footprints overlap each other if the laser beam has not moved enough in between two laser shots. The same portion of scenery is scanned twice. To avoid a loss in time-efficiency and to improve the robustness with respect to the noise, the average of the two overlapping areas is computed. The resulting visualization panel, of the *Zig-Zag scanning*, is shown by Figure 4.7 where the characteristic Z-shaped pattern is observed in the middle picture.

Figure 4.7. Simulation: Zig-Zag scanning.

4.3   Workspace Indications

The workspace of Matlab is also used to display information about the simulation which has been run.

When the *pixel simulation* is run, the user finds the distance computed. The result should be compared with the target range: the closer to the target range the result is, the more accurate it is!

When the *LADAR image generation* has been run, indications about resolutions are given (footprint size, subareas size, ...). Moreover, two mean square errors (MSE) are computed:

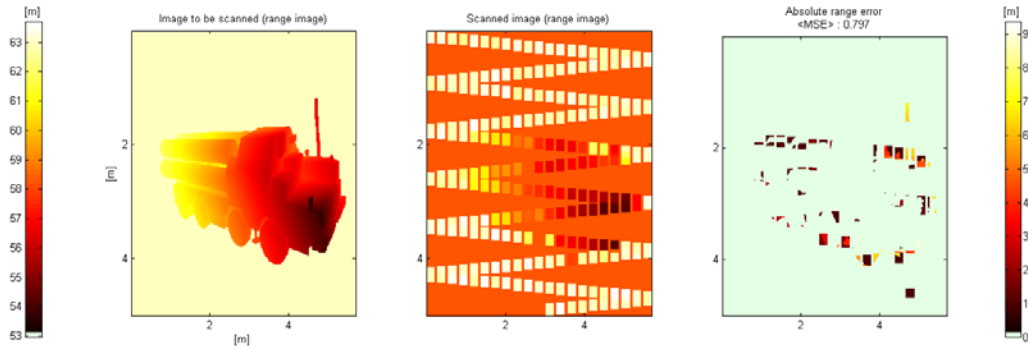1. The "auto - mean square error" represents the error between the LADAR image generated and the original 2D range image of the target (it is the error displayed in figures 4.6 and 4.7). This is the reference error related to the target itself.

2. The "cross - mean square error" represents the error between the LADAR image generated and the 2D range image chosen in the library (as detailed in Section 4.1.2). The library contains 2D range images of several targets, including the target being scanned. The "cross - mean square error" is computed using one of these images. Note that if the 2D range image of the target being scanned is selected, the result is the same as the one obtained with the "auto - mean square error".

Comparing the "auto - mean square error" to the "cross - mean square error" is a first means to identify the similitudes between two objects. Working with a not too high noise level, one expects the relation:

$$\text{"auto - mean square error"} \leq \text{"cross - mean square error"}$$

Equality occurs when the target selected in the library is the same than the one being scanned. This can be interpreted as a *primary* target recognition method.

Part III

Results & Reflections

Chapter 5

Simulation Results

The LADAR simulation has been developed to support system engineering studies. To do so, it produces simulated range images under a wide variety of conditions. This simulator is of good help in understanding how the different phenomena affect the final images. In this section, some series of simulations are presented. To facilitate the interpretations and to be easily understandable, only one parameter at a time is changed. The simulations illustrate: the performances of the detection algorithms with the noise addition; the relation between the footprint size and the resolution; the sampling rate and its consequences on the range accuracy; the Zig-Zag scanning.

5.1 Classical LADAR Image

All the following paragraphs are based on the original LADAR image seen in Figure 5.1. It shows a classical LADAR image generation with default parameters.
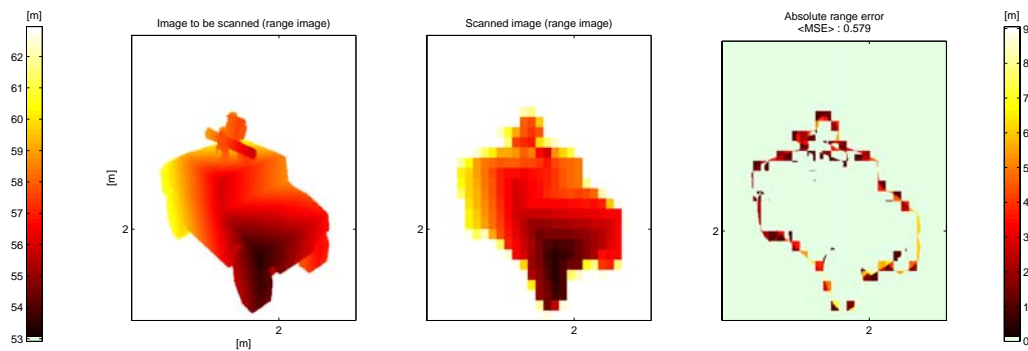
Figure 5.1. Classical LADAR image.

In this ideal case, one may note that there is no noise added (this is studied in Section 5.2). Moreover, the sampling frequency at the receiver is high (1000 MHz) so that it does not influence the result. The pulse detection algorithm used is the CFD algorithm.

5.2   Noise Addition and Detection Algorithms

Figure 5.2 illustrates the performances of two detection algorithms in presence of noise. From Section 5.1, only the SNR has been changed and its value is 3.
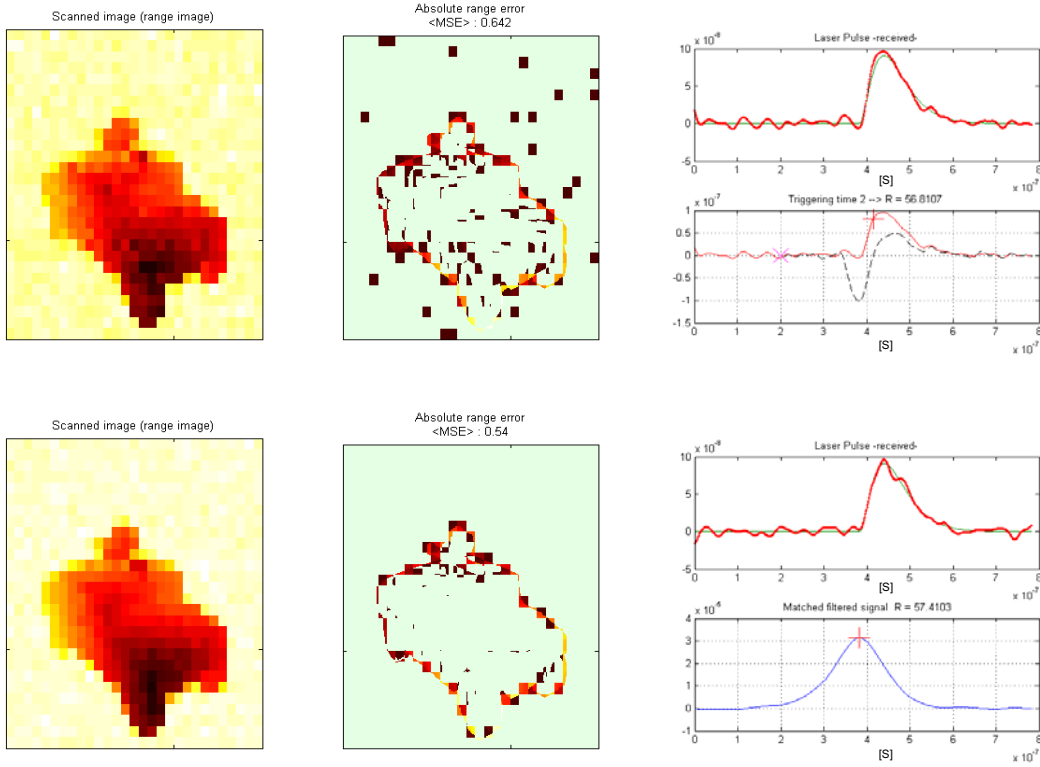
Figure 5.2. LADAR images with CFD and matched filter.

On one hand, the 1st row of graphics is obtained with the *CFD algorithm*. On the other hand, the 2nd row of graphics is obtained with the *matched filter algorithm*. The curves on the right side of the figure are generated thanks to the *pixel simulation* to detect a surface at 57.55 m.

From these results, the matched filter appears to be more efficient than the *CFD algorithm*. This comes from the fact that the matched filter is not affected by the Gaussian noise by construction. It is a robust method with

respect to white noise. This is shown by the signals in Figure 5.2. In the CFD method, the timer is trigged using the received pulse which is distorted by the noise. As a consequence, the time and then the distance computed are not accurate. On the other hand, the output of the matched filter is not modified by the noise addition. The maximum can be detected without any extra error and leads to a more accurate result than in the CFD method. This interpretation becomes more and more true for increasing noise levels.

5.3 Footprint Size and Resolution

Figure 5.3 shows two images with two different divergence angles (all the other parameters are the same than in Figure 5.1).
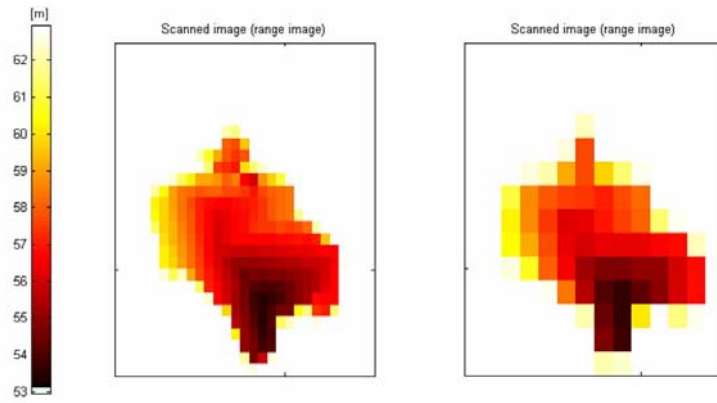
Figure 5.3. LADAR images with divergence angles of 0.1 deg and 0.2 deg.

The footprint size can be modified by adjusting the laser beam divergence. This permits finding a compromise between resolution and processing time. Indeed, to the footprint size corresponds directly the size of the pixels in the LADAR image. Increasing the divergence increases the footprint size and then deteriorate the LADAR image resolution.

5.4 Sampling Frequency and Range Accuracy

Figure 5.4 is an illustration of the consequences of the sampling occurring at the receiver stage. The 1st image is the same than the LADAR image of Figure 5.1 where the sampling frequency is 1000 MHz. This frequency has been decreased to 100 MHz to generate the 2nd picture.

The influences of the sampling frequency on the range accuracy appear obvious in this picture. Both pictures have the same cross-range resolution (x
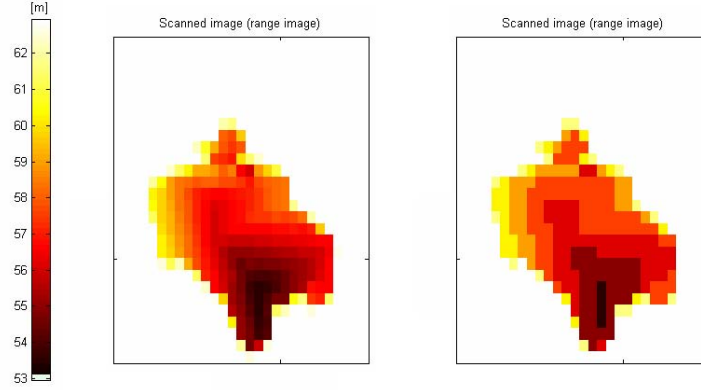
Figure 5.4. LADAR images with $F_s = 1000\ Hz$ and $F_s = 100\ Hz$.

and y). However, the range dimension (z), represented by the color, is lower while using a lower sampling frequency. This phenomenon is represented by the apparition of larger areas with the same color in the 2nd picture.

5.5   Zig-Zag Scanning

Figure 5.5 shows an example of Zig-Zag scanning. The parameters used to carry out the scanning are: $PRF = 2000\ Hz$, $f_{sc} = 100\ Hz$, $V = 50\ m/s$, *flight distance* $= 3\ m$ and $FOV = 3$ deg. The settings have been chosen so that no overlapping occurs. Moreover, this result shows the necessity of increasing the number of cells at the receiver in order to obtain a better image with more pixels.
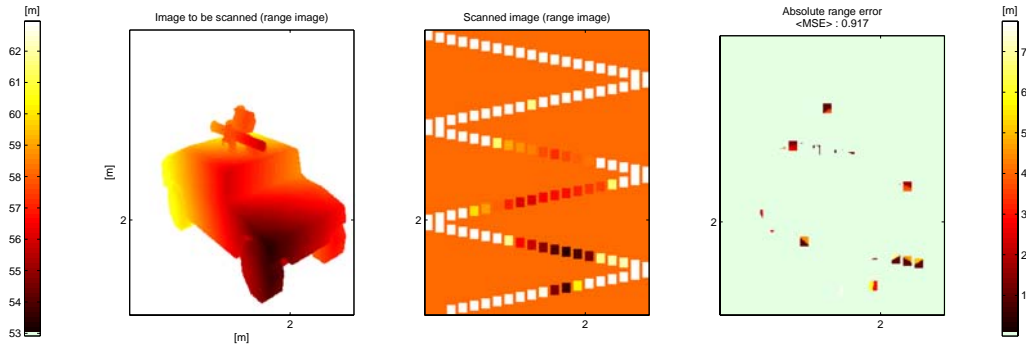
Figure 5.5. LADAR image using Zig-Zag scanning.

Furthermore, this LADAR image brings up the question of target recogni-

tion using discontinuous images. In Section 4.3, a primary target recognition method is described which implies the computation of MSEs. In the Zig-Zag scanning case, the MSEs are computed on the whole images as before. However, two others extra MSEs are computed based on the processed pixels only. It provides an alternative criteria for the target recognition using discontinuous images.

5.6   Conclusion

The simulations presented in this section give an overview of the possibilities of the simulator. This is only a selection which is, according to the author, easily understandable by the reader. Nevertheless, the LADAR simulation offers a wider range of possibilities which is left to be discover by the future user. From these examples, one sees that it is possible to build a modelling tool for the laser target imaging which can predict the performances and results from LADAR systems. The combination of the laser images with the simulated waveforms provides a powerful tool permitting to carry out detailed analysis.

Chapter 6

Reflections

6.1 Conclusions

From the laser source to the optical receiver, the simulator which has been developed models various stages of the whole LADAR imaging process. The modular nature of the simulator permits to reproduce different conditions thanks to the wide choice in parameters. The breaking of the pulse into components and the use of 2D range images were the keys to success. Thus, the simulation can generate reflected pulses for any target shapes. This modular simulation associated to its powerful graphical interface represents a primary engineering software. This tool will permit to assist the design of future LADAR systems and to carry out performances tests.

A such modular simulator could be of good use in the following applications:

- LADAR UAV platforms using the 3D mapping capabilities to acquire 3D models of land and building.

- UAV 3D scanning LADAR for target identification.

- LADAR for autonomous vehicle guidance, hazard avoidance and obstacle detection.

- LADAR terrain mapping for space exploration and autonomous vehicle navigation.

- Studies of advanced LADAR missile seekers and intelligent proximity fuzes (guided missiles of type LOCAAS or E-COM).

The simulation program presented in this report is as a first step in the direction of future full simulation softwares for 3D laser imaging. A suggestion would be to converge with the work done by Ove Steinvall in [2] and use the

model layout[1] presented in Figure 6.1 as a reference for the future developments of 3D laser imaging simulators.
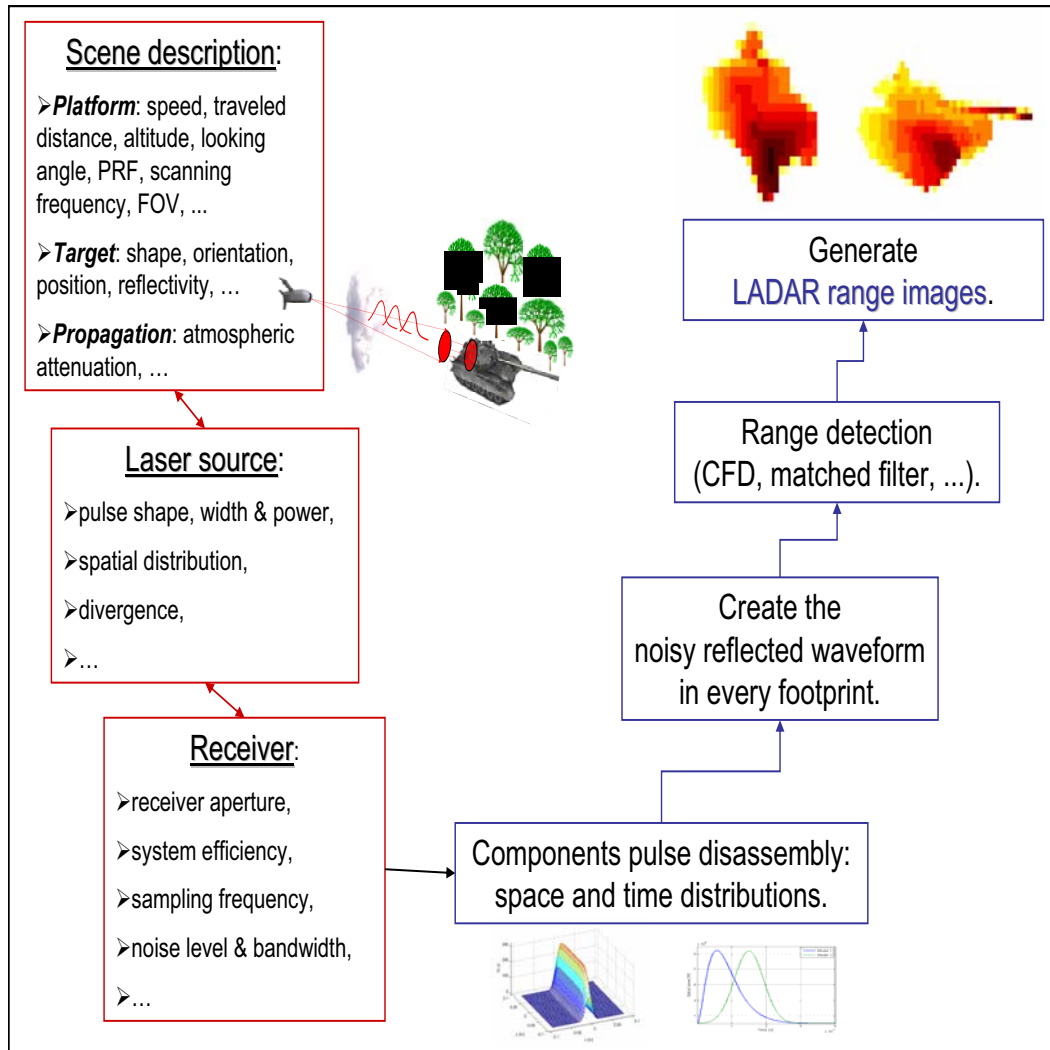

Figure 6.1. Development of a 3D LADAR imaging simulator.

---

[1]inspired from the work of Ove Steinvall found in [2] and that I would never thank enough for his "indirect" contribution.

6.2 Suggested Future Work

The completed work represents the first step in the direction of a thoroughgoing simulator. Hence, every stage of the simulation could undergo optimizations[2] which would make it closer to the reality and improve its accuracy.

Above all, the LADAR simulation would required detailed validations of the provided information. Quantitatively, the entire simulation could be subject to extensive verifications under predetermined conditions. Qualitatively, the simulation results may for example be compared with laboratory tests using real devices and targets.

Afterwards, every module could be improved by complexifying the models used. The simple atmospheric attenuation coefficient may be substituted by an advanced modelling of the atmospheric effects: beam broadening, intensity fluctuations and aerosol attenuation. The references [7, 10, 11] provide detailed theory about atmosphere modelling.

The reflection on the target may for example be developed by taking into account the bidirectional reflection density function ($BRDF$). The $BRDF$ describes how the reflected beam spreads into different angles in relation with the surface's properties. This gives a more realistic representation of the phenomenon as seen in [1, 7, 8]).

As a consequence, the target modelling would include more information than the one already contained in the range images (that is to say the distance from the laser source). They also ought to contain the surface characteristics (slope, material) in each pixel. Another point might be the implementation of a dynamic range image generation. This would permit to work with the exact view of the scenery in corresponding to the flight conditions at every moment.

Thus, an important part would be to focus on the signal and image processing. Indeed, the pulse detection in presence of noise as well as the feature extraction from LADAR pictures are two wide fields of ongoing research. Advanced work could be carried out in these directions using [7, 17, 18, 19].

Finally, the current work could be extended by implementing some other functionalities. For example, the number of receiver's cells may be increased and thus a whole array of detectors could be used, see [19] for discussions about the 3D focal plane array. Furthermore, the detection method may be expanded by implementing a coherent detection method based on the decription given in [10].

The way leading to an exhaustive simulator might be tediously long.

---

[2]fortunately for the reader, only the paramount elements of the boundless list are presented here.

Acknowledgements

References

[1] O Steinvall and T Carlsson. *Three-dimensional laser radar modelling.* Proceedings of SPIE Vol. 4377, 2001.

[2] O Steinvall. *Waveform simulation for 3-d sensing laser radar.* FOA-R–00-01530-612,408–SE, 2000.

[3] Q Zheng, S Z Der, and H I Mahmoud. *Model-based target recognition in pulsed ladar imagery.* IEEE, 1057-7149/01, Vol. 10 No. 4, 2001.

[4] S Z Der, B Redman, and R Chellappa. *Simulation of error in optical radar range measurements.* Optical Society of America, 0003-6935/97/276869-06, Vol. 36 No. 27, Applied Optics, 1997.

[5] E Hetch. *Optics.* Pearson Education International, 2002.

[6] ZEMAX user's guide. *ZEMAX, optical design program.* chap. 12, p359-360, 2006.

[7] T Carlsson, O Steinvall, and D Letalick. *Signature simulation and signal analysis for 3-D laser radar.* FOI-R–0163–SE, ISSN 1650-1942, 2001.

[8] O Steinvall. *Effects of target shape and reflection on laser radar cross sections.* Optical Society of America, 0003-6935/00/244381-11, Vol. 39 No. 24, Applied Optics, 2000.

[9] Encyclopedia of laser physics and technology. www.rp-photonics.com.

[10] Accetta and Shumaker. *The infrared and electro-optical systems handbook.* Vol. 6 Active electro-optical systems, ISBN 0-8194-1072-1, 1993.

[11] O Steinvall. *Theory for laser systems performance modelling.* FOA-R–97-00599-612–SE–SE, 1997.

[12] R Telgarsky, M C Cates, C Thompson, and J N Sanders-Reed. *High fidelity LADAR simulation.* SPIE 5412, 2004.

[13] W J Smith. *Modern optical engineering, the design of optical systems.* R
     E Fischer and W J Smith, 1990.

[14] A V Jelalian. *Laser radar systems.* Artech house, 1992.

[15] E P Baltsavias. *Airborne laser scanning: basic relations and formulas.*
     ISPRS Journal of Photogrammetry and Remote Sensing 54, p199-214,
     1999.

[16] O Steinvall, D Letalick, U Söderman, L Ulander, and A Gustavsson.
     Laser radar for terrain and vegetation mapping. FOI-R–0232–SE, 2001.

[17] P Andersson. *Automatic target recognition from laser radar data.* FOI-
     R–0829–SE, 2003.

[18] Å Persson. *Extraction of individual trees using laser radar data.* FOI-R–
     0236–SE, 2001.

[19] O Steinvall, T Carlsson, C Grönwall, H Larsson, P Anderson, and
     L Klasén. *Laser based 3D imaging new capabilities for optical sensing.*
     FOI-R–0856–SE, 2003.

Appendix A

Parameter Description

The following figures (numbers A.1, A.2, A.3, A.4 and A.5) contain the m-file displayed after pressing the help-button on the GUI. This file stands for a help file, giving brief explanations about every item of the GUI front panel. They are listed at the beginning of the file and are presented in alphabetical order.

```matlab
% README is a "help" file. SIMULATOR_LADAR_GUI is the graphical user
% interface of the LADAR proximity fuse simulation. Here is the description
% of its parameters.
% Run the simulator by running the m-file "SIMULATOR_LADAR_GUI.m".

%%%%%%%%%%%%%%%%%%%%%%%%%%%%%%%%%%%%%%%%%%%%%%%%%
% Developed with the Matlab R2006a version 7.2.0.232
%%%%%%%%%%%%%%%%%%%%%%%%%%%%%%%%%%%%%%%%%%%%%%%%%

% !!!NOTE!!!

% If you want to use your own 2D range image describing your target:
%
% *** store your 2D range image (typically 500x500) in the folder "Images".
% The format of that image MUST be ".bmp".
% *** display the list of personal 2D range images. To do so, select the
% entry "personal_images_list" in the pop-up menu corresponding to the
% looking angle parameter.

%%%%%%%%%%%%%%%%%%%%%%%%%%%%%%%%%%%%%%%%%%%%%%%%%%%
%
%
% Copyright 2006-2007
% Eric Blanquer
%
%%%%%%%%%%%%%%%%%%%%%%%%%%%%%%%%%%%%%%%%%%%%%%%%%%%

% The descriptions are given as the following template:

    GUI_name_parameter_____code_name_parameter //type of the control
        % action and consequences.
        % Short description of the parameter.
        units [ ]

% Here is the alphabetical list of the parameters:
    altitude_____height //edit
    atmospheric_attenuation_____alpha //edit
    B_____B //edit
    ceil_range_____ceil_range //edit
    Detection_algorithm_____detect //popupmenu
    divergence_angle_____thetay_fwhm //edit
    f_sc_____f_sc //edit
    Flight_distance_____dim_a //edit
    FOV_____dim_b //edit
    Fs_____Fs //edit
    FWHM_____FWHM //edit
    looking_angle_____looking_angle //edit
    nsa_____nsa //edit
    PRF_____PRF //edit
    Pulse_power_____I0 //edit
    Pulse_shape_____shape_num //popupmenu
    receiver_aperture_____r_aperture //edit
    SNR_____FACTOR //edit
    SNR_slider_____noise_param2 //slider
    system_efficiency_____eta_syst //edit
    target_reflectivity_____rho //edit
    V_____V //edit


%%%%%%%%%%%%%%%%%%%%%%%%%%%%%%%%%%%%%%%%%%%%%%%%%%%%%

altitude_____height //edit
        % set height and display the distance to the ground. height is the
```

Figure A.1. Help file 1/5.

```
                    % altitude of flight of the platform.
                    units [m]


atmospheric_attenuation_____alpha //edit
                    % set alpha and display the atmospheric attenuation graph. alpha is
                    % the atmospheric attenuation coefficient representing the
                    % attenuation due to the atmosphere with the expression:
                    % exp(-2*alpha*R), R being the distance from the source.
                    units [XXX]


B_____B //edit
                    %   set B and display the corresponding Bode diagram of the filter.
                    %   B is the bandwidth of the system from the receiver point of
                    %   view. A low-pass filtering, with cutting frquency B, is applied
                    %   to all the in-coming signals including the noise.
                    units [MHz]


ceil_range_____ceil_range //edit
                    % set ceil_range. ceil_range is the distance after which the
                    % detection is enabled (nothing can be detected from the laser
                    % source to the distance ceil_range).
                    units [m]


Detection_algorithm_____detect //popupmenu
                    % select the pulse detection method. The user can use among 3
                    % different pulse detection methods:
                    %
                    % 1) CFD: Constant Fraction Discrimination. Detect the received
                    %  pulse using the zero crossing of a S-shape pulse obtained from
                    %  the received pulse.
                    %
                    % 2) CFD 50%: Constant Fraction Discrimination. Detect the received
                    %  pulse using the zero crossing of a S-shape pulse obtained from
                    %  the received pulse. Then, use a 50% leading edge detection.
                    %
                    % 3) Matched filtering: use a match filter with its impulse
                    %  response equal to the time reverse laser pulse shape.


divergence_angle_____thetay_fwhm //edit
                    % set thetay_fwhm thetax_fwhm and display the grid of the spacial
                    % distribution. thetay_fwhm is the biggest divergence angle of the
                    % laser source modelled as a slit. The other divergence angle is
                    % equal to 1/10 of the biggest divergence angle.
                    units [degree]


f_sc_____f_sc //edit
                    % set f_sc. f_sc is the scanning frequency used in the Zig-Zag
                    % scanning. The corresponding period, 1/f_sc, is defined as the
                    % time to draw one line (from left to right OR from right to left).
                    units [Hz]


Flight_distance_____dim_a //edit
                    % set dim_a, the travelled distance. dim_a is the distance
                    % travelled by the platform during its scanning. This distance is
                    % linked with the platform' speed V and represents also the length
                    % of the final LADAR image.
```

Figure A.2. Help file 2/5.

```
        units [m]


FOV_____dim_b //edit
        % set dim_b, the FOV. dim_b is the Field Of View of the LADAR
        % system. It is defined by the angular aperture of the scanning.
        % (The scanning is done on a transversal angle from -dim_b/2 to
        % +dim_b/2). It influences the width of the final LADAR image.
        units [degree]


Fs_____Fs //edit
        % set Fs and plot the sampled pulse. Fs is the sampling frequency
        % used at the receiver in the pulse acquisition. This is done to
        % simulate the A/D conversion.
        units [MHz]


FWHM_____FWHM //edit
        % set FWHM and plot the pulse. FWHM is the Full Half Width Maximum
        % of the pulse and is used to define the duracy of the pulse.
        units [ns]


looking_angle_____looking_angle //popupmenu
        % set looking_angle, display the distance to the target and the
        % suitable 2D range images lists.
        % looking_angle is the angle of view of the laser system taken
        % from the horizontal. The value 90 corresponds to a vertical
        % scanning (directly under the plateform).
        units [degree]


nsa_____nsa //edit
        % set nsa and display the grid of the spacial distribution. nsa is
        % the number of sub-areas constituting one laser footprint. It
        % represents the grid used to describe the spacial distribution of
        % the power.
        units [XXX]


PRF_____PRF //edit
        % set PRF. PRF is the Pulse Repetition Frequency of the LADAR
        % system. It represents the frequency used to send laser pulses in
        % the Zig-Zag scanning.
        units [Hz]


Pulse_power_____I0 //edit
        % set I0 and plot the pulse. I0 is the coefficient used to change
        % the power of the laser pulse.
        units [W]


Pulse_shape_____shape_num //popupmenu
        % select the pulse shape and plot the pulse. The user can choose
        % between 2 different pulse shapes corresponding to 2 different
        % mathematical expressions:
        % 1)
        %  tau = FWHM/3.5;
        %  pulse = (t/tau).^2.*exp(-(t/tau));
        % 2)
        %  pulse = exp(-4*log(2)*((t-1.5.e-7)/FWHM).^2);
```

Figure A.3. Help file 3/5.

```
receiver_aperture_____r_aperture //edit
        % set r_aperture. r_aperture is the radius aperture of the
        % receiver.
        units [m]


SNR_____FACTOR //edit
        % set FACTOR and plot the noisy pulse. FACTOR is the SNR of the
        % received pulse. Changing this value allows the user to simulate
        % different amount of random noise (zero mean noise).
        units [XXX]


SNR_slider_____noise_param2 //slider
        % set FACTOR, display the value and plot the noisy pulse. This
        % slider is another mean to change the SNR of the received pulse.
        % See SNR_____FACTOR //edit for the details.
        units [XXX]


system_efficiency_____eta_syst //edit
        % set eta_syst. eta_syst is the efficiency of the whole system. The
        % value is in the interval [0,1].
        units [XXX]


target_reflectivity_____rho //edit
        % set rho. rho is the hemispherical reflectivity of the target and
        % represents the percentage of reflected laser light. The value is
        % in the interval [0,1].
        units [XXX]


V_____V //edit
        % set V. V is the speed of the platform in the air and is taken
        % into account in the Zig-Zag scanning.
        units [m/s]


%%%%%%%%%%%%%%%%%%%%%%%%%%%%%%%%%%%%%%%%%%%%%%%%%%
 
%%%%% Push buttons:

    RUN_LADAR_image_____run //button
        % desactivate the main figure, start the RUNNING mode, clear the
        % second figure, run the simulation case selected.


    pixel_simulation //button
        % desactivate the main figure, start the RUNNING mode, run the
        % pixel simulation. It simulates the signals obtained for one laser
        % shot for one pixel located a the ground distance.


    STOP_____stop //button
        % stop the on going simulation and display a stop message on the
        % workspace.


    Close_simu_____close //button
        % close the simulation.
```

Figure A.4. Help file 4/5.

```
    Reset_simu_____reset //button
        % close and open again the simulation with the default parameters.


    Help //button
        % display the help file of the GUI.


Simulation_case_____selcbk //buttongroup
        % select the case to be simulated. The user can choose between:
        %
        % 1) Ideal case: v, f_sc and PRF are NOT taken into account in this
        %  simulation. It is an ideal case where the foot print pattern has
        %  a perfect match with the scanned area. The foot prints do not
        %  overlapp or are not disjoint. The scanning covers the whole
        %  image. It is based on a one cell receiver.
        %
        % 2) Zig-Zag scanning: this is the realistic scanning in which v,
        %  f_sc and PRF are taken in to account. In case of overlapping
        %  foot prints, the average is computted on the common area. It is
        %  based on a one cell receiver.


%%%%%%%%%%%%%%%%%%%%%%%%%%%%%%%%%%%%%%%%%%%%%%%%%%%
```

Figure A.5. Help file 5/5.

Appendix B

Creation of the source diode model (m-file)

The following figures (numbers B.1 and B.2) stand for the m-file containing the Matlab function which creates the source diode model used in the simulation. The example provided in the description of the function is a stand alone example and can be run by the reader once the m-file has been reproduced.

```matlab
function [I_x_y, L] = source_diode_xy_02(R, nsa)

% SOURCE_DIODE_XY_02 creates the NORMALIZED IRRADIANCE of the source diode
% model in the x and y coordinate system at a target distance R. The
% target range is take into account in the function profile (R dependent)
% since the profile is attenuated by a factor R^2.
%
% [I_x_y] = source_diode_xy_02(R, nsa).
%
% source_diode_xy_02(R, nsa), plots the normalized irradiance.
%
% ***INPUTS***
% R : target range.
% nsa : number of sub-areas constituting the footprint.
%
% ***OUTPUTS***
% I_x_y : IRRADIANCE of the source diode model at a target distance R.
%
% Example:
% global thetay_fwhm
% global thetax_fwhm
% thetay_fwhm = 0.2;
% thetax_fwhm = thetay_fwhm/10;
% source_diode_xy_02(50, 2000);
%
% See also Simulation_051, Simulation_071, pixel_shot
%
% Copyright 2006-2007
% Eric Blanquer
% ericblanquer@hotmail.com
%
%%%%%%%%%%%%%%%%%%%%%%%%%%%%%%%%%%%%%%%%%%%%%%%%%%%%%%

%% Function
global thetax_fwhm
global thetay_fwhm

Gx = 1; %SuperGaussian coefficient, must be >1
Gy = 5; %SuperGaussian coefficient, must be >1

if Gx < 1
    error('ERROR: Gx must be >= 1')
else
    if Gy < 1
        error('ERROR: Gy must be >= 1')
    else
        %definition of the footprint dimensions using the FWHM angles:
        l1 = 2*R*tan( (thetax_fwhm*pi)/(2*180) );
        l2 = 2*R*tan( (thetay_fwhm*pi)/(2*180) );
        %take the largest dimension to create a SQUARE shaped pixel:
        L = max(l1, l2);
        L = ceil(L*1000)/1000;

        sr = L/sqrt(nsa); %spatial resolution
        if nsa < 50
```

Figure B.1. Source diode model 1/2.

```matlab
        error('ERROR: choose a bigger nsa!')
    elseif nsa > 10000
        error('ERROR: choose a smaller nsa!')
    end

    xy = - L/2:sr:L/2; %xy spatial variable

    %change of variables:
    thetax = (xy/R - (1/3)*(xy/R).^3) / (pi/180);
    thetay = (xy/R - (1/3)*(xy/R).^3) / (pi/180);
    %angle conversion:
    alphax = (2/log(2))^(1/(2*Gx))*(1/2)*thetax_fwhm;
    alphay = (2/log(2))^(1/(2*Gy))*(1/2)*thetay_fwhm;
    %source diode model, matrix creation:
    I_thetax = exp(-2*((thetax/alphax).^(2*Gx))); %row
    I_thetay = exp(-2*((thetay/alphay).^(2*Gy))); %row
    I_x_y = 1/R^2 * I_thetax' * I_thetay;
    %Normalization:
    I_x_y = I_x_y / ( sum(sum(I_x_y))*sr^2 );
    %Transpose to match to the xy axis description:
    I_x_y = I_x_y';
    end
end

%% Plot

if nargout == 0
    %find Maximum:
    M = max(max(I_x_y));
    mesh(xy, xy, I_x_y);
    title(['Normalized irradiance - distance: ', num2str(R)])
    xlabel('x [m]'), ylabel('y [m]')
    axis([-0.6*L 0.6*L -0.6*L 0.6*L 0 M])
end
```

Figure B.2. Source diode model 2/2.

Appendix C

Pulse detection: the CFD algorithm (m-file)

The following figures (numbers C.1, C.2 and C.3) stand for the m-file containing the Matlab function which runs the CFD algorithm. Actually, both the CFD and the CFD 50% algorithms are contained in this m-file. The example provided in the description of this function provides the signals related to the CFD algorithm only.

```matlab
function [timepeak, valpeak] = CFD(t, pulse, FWHM, ceil_range, trigger_time1)

% CFD returns the index and the value of the pulse's point corresponding to
% the main zero crossing of the S-shape signal: using the CFD (Constant
% Fraction Discrimination) method. Setting detect to 'CFD_50', modify the
% CFD method by applying a CFD & 50%leading edge detection.
%
% [indexpeak, peak] = CFD(t, pulse, FWHM, ceil_range).
%
% [indexpeak, peak] = CFD(t, pulse, FWHM) uses ceil_range = 0.
%
%
% CFD(t, pulse, FWHM, ceil_range), displays a plot of the different signals.
%
% ***INPUTS***
%   t : vector time used to create the pulse
%   pulse : the laser pulse
%   FWHM : the FWHM of the pulse
%   ceil_range : an object in between the source and ceil_range will NOT be
%   detected. It is represented by the magenta cross on the plot.
%
% ***OUTPUTS***
%   indexpeak : peak index (trigger time)
%   peak : peak value ("maximum") represented by the red cross on the plot
%
% Example (requires crossing.m):
% FWHM = 100*1.e-9;
% t = (1:400)*1.e-9;
% tau = FWHM/3.5;
% pulse = (t/tau).^2.*exp(-t/tau) * 1/(2*tau);
% CFD(t, pulse, FWHM);
%
% See also crossing, range
%
% Copyright 2006-2007
% Eric Blanquer
% ericblanquer@hotmail.com
%
%%%%%%%%%%%%%%%%%%%%%%%%%%%%%%%%%%%%%%%%%%%%%%%%%%%%%%%

%% Function
global detect

%Identify the temporal resolution:
delta = t(2) - t(1);

%Value of the time shift used to create the 2nd signal:
shift = ceil(FWHM/2 / delta);

%Set the ceil range to zero by default:
if nargin == 3 || ceil_range < 0.1
   ceil_range = eps;
end

%Derived the corresponding ceil time:
```

Figure C.1. CFD algorithm 1/3.

```matlab
if nargin == 3
    ceil_time = ceil_range/299792458;
else
    ceil_time = ceil_range/299792458 + trigger_time1/2;
end

ceil_time = 2*ceil_time; %flight time of the pulse to the ceil_range
ceil_detection = ceil(ceil_time/delta); %ceil's index

%The detection is disabled untill the ceil_detection:
pulse_c = [pulse(ceil_detection:end) zeros(1, ceil_detection-1)];
t_c = [t(ceil_detection:end) ((1+length(t)):(ceil_detection-1+length(t)))*delta];

%The pulse is shifted of "shift" and mirrored:
pulse_s = -[pulse_c(shift:end) zeros(1, shift-1)];

%Addition with the original pulse, S-shape resulting signal:
pulse_out = pulse_c + pulse_s;

%Use of the function 'crossing' to get the zero crossing index:
[ind] = crossing(pulse_out,t_c); %all the zero crossings

%MPoints of the original pulse corresponding to the zero crossings:
timepeaks = t_c(ind);
valpeaks = pulse_c(ind);

%Select the pulse's point corresponding of the main zero crossing of the
%S-shape signal:
[valpeak, indtimepeak] = max(valpeaks);
timepeak = timepeaks(indtimepeak);

%CFD & 50%leading edge, identical to CFD but one computes the point at 50%
%of the pulse's point corresponding of the main zero crossing of the
%S-shape signal:
if strcmp( detect, 'CFD_50' ) == 1
    indextimepeak = find(t == timepeak);
    pulse50 = pulse(1:indextimepeak);
    t50 = t(1:indextimepeak);

    [ind50] = crossing(pulse50,t50, 50/100*valpeak);

    timepeaks50 = t(ind50);
    valpeaks50 = pulse(ind50);

    valpeak50 = valpeaks50(length(valpeaks50));
    timepeak50 = timepeaks50(length(timepeaks50));

    timepeak = timepeak50; valpeak = valpeak50;
end

%% Plots

if nargout == 0
    plot(t, pulse, 'r')
    hold on
```

Figure C.2. CFD algorithm 2/3.

```
    grid
    %plot(t_c, pulse_s, 'g')
    plot(t_c, pulse_out, 'k--')
    plot(timepeak, valpeak, 'r+', 'MarkerSize',20)
    plot(t_c(ceil_detection)/2, 0, 'mx', 'MarkerSize',20)
    hold off
    V = axis;
    V(2) = t(end);
    axis(V);
end
```

Figure C.3. CFD algorithm 3/3.

Index

The Author

Eric Blanquer concludes with this Master of Science Thesis a double degree program. Thanks to international agreements between France and Sweden, he is about to receive two diplomas: the Master of Science in Systems Engineering from KTH (the Royal Institute of Technology of Stockholm, Sweden) and the Master of Science in electrical engineering from INPG (the Grenoble Institute of Technology, France).

His studies include automatic control, signal processing, system study, simulation, and modelling.

✉ ericblanquer@hotmail.com

📱 +46 70 474 95 67